

Singular Vectors of Attention Heads Align with Features

Gabriel Franco¹ Carson Loughridge¹ Mark Crovella^{1,2}

Abstract

Identifying feature representations in language models is a central task in mechanistic interpretability. Several recent studies have made an implicit assumption that feature representations can be inferred in some cases from singular vectors of attention matrices. However, sound justification for this assumption is lacking. In this paper we address that question, asking: why and when do singular vectors align with features? First, we demonstrate that singular vectors robustly align with features in a model where features can be directly observed. We then show theoretically that such alignment is expected under a range of conditions. We close by asking how, operationally, alignment may be recognized in real models where feature representations are not directly observable. We identify *sparse attention decomposition* as a testable prediction of alignment, and show evidence that it emerges in a manner consistent with predictions in real models. Together these results suggest that alignment of singular vectors with features can be a sound and theoretically justified basis for feature identification in language models.

1. Introduction

Improving the interpretability of language models is critical, e.g., to build a foundation for improving model safety (Anwar et al., 2024). A central task in interpretability is the identification of *feature representations* – the elucidation of how models represent the concepts that they manipulate.

There is now considerable evidence that many concepts in language (and other) models are represented as directions in one-dimensional or low-dimensional subspaces (Elhage et al., 2022; Olah et al., 2020; Mikolov et al., 2013; Alain & Bengio, 2018; Park et al., 2023; Gurnee & Tegmark,

¹Department of Computer Science, Boston University, Boston, USA ²Faculty of Computing & Data Sciences, Boston University, Boston, USA. Correspondence to: Gabriel Franco <gvfranco@bu.edu>.

2024; Gurnee et al., 2023; Marks et al., 2024; Levy & Geva, 2025; Engels et al., 2025; Kantamneni & Tegmark, 2025; Hernandez et al., 2024). This has been termed the *linear representation hypothesis* (LRH) (Park et al., 2023; Elhage et al., 2022). However, reliably identifying the actual linear representations used by models in arbitrary settings is still an unsolved problem. That is, the LRH suggests that model activations can be conceived as additive sums of features, but finding the proper decomposition of a particular activation into its constituent features is still an enormous challenge.

In this regard, a number of studies have examined the weights of attention heads, in particular decomposing those weights using singular value decomposition, as a framework for studying feature representations (Merullo et al., 2024; Ahmad et al., 2025; Pan et al., 2024; Franco & Crovella, 2024; 2025). These studies suggest a surprising relationship: **features used by an attention head tend to be aligned with its singular vectors.**¹ This does not require each feature to be one-dimensional; for example, a feature may lie in a low-dimensional subspace spanned by a small set of singular vectors. But in fact, many features appear to be one-dimensional and approximately in the same direction as a single singular vector (Merullo et al., 2024; Franco & Crovella, 2024).

The alignment of singular vectors with features presents a natural and powerful tool for interpretability. This is because the singular vector basis of a head then provides a comprehensible and tractable search space for extracting features from model activations. Projecting a model activation onto the various subspaces defined by a head’s singular vectors defines a discrete set of candidate features. These candidate features can then be analyzed in various ways, e.g., for causal impact on task performance.

Thus, the phenomenon of singular vector–feature alignment needs further exploration. Hence, our motivating question:

¹By singular vectors of an attention head, we mean the singular vectors of the head’s QK matrix $\Omega = W_Q^\top W_K$. Details are introduced below.

Research Questions

When features are represented linearly, under what conditions will the singular vectors of attention head matrices align with those features? Can we understand singular vector-feature alignment theoretically, and find evidence of alignment in real models?

Note that there are really two surprises here. The first is that any singular vector aligns with any feature at all. But a second surprise is that, in order for multiple features to align with corresponding singular vectors, the features must be nearly orthogonal (since singular vectors are themselves orthogonal). A complete study necessitates understanding both phenomena: both the single-feature case and the multi-feature case. Together we refer to these two phenomena as *singular vector–feature (SVF) alignment*.

To explore these phenomena, we use a combination of toy-model studies and theory. We illustrate and explore SVF alignment using a toy model similar to (Elhage et al., 2022), which we extend to include an attention head. We then present theorems that confirm the observed SVF alignment, and establish conditions under which it provably occurs. We then use these observations to formulate testable predictions that are implied by SVF alignment, and confirm that those predictions hold in both toy and real models (GPT-2 and Pythia).

We summarize our contributions as follows. Our base assumptions are that features are linearly represented and activations are formed by summing features. Then:

Main Results

- SVF alignment arises robustly in a setting where heads attend to specific feature pairs.
- The top singular vectors of a head align with the feature pair most important for computing attention.
- Features orthogonalize to minimize interference, allowing for SVF alignment across multiple feature pairs.
- SVF alignment implies a testable prediction called *sparse attention decomposition*, which we confirm arises in real models.

2. Background

The notion of *feature* has been given varying definitions in the literature. Here, we consider a feature to be a geometrically *and* semantically consistent representation that has some functional role in the model. Geometric consistency is realized by treating features as vectors, and semantic consistency is realized by hypothesizing that attention heads compute attention values as a function of which features are

present in tokens. This view encompasses both the geometric properties surfaced by linear probes and SAEs, as well as the semantic properties required by causal analysis.

SVF alignment refers to a situation in which a feature, represented as a vector, has a high cosine similarity to a singular vector of an attention head’s QK matrix. We denote the QK matrix Ω , defined as $W_Q^\top W_K$, and the left and right singular vectors of Ω are the columns of U and V as given by the SVD of Ω , ie, $\Omega = U\Sigma V^\top$.

SVF alignment has been an implicit or explicit assumption in a number of recent studies. The authors in (Merullo et al., 2024) find that inter-layer communication in models can be understood as taking place in low-rank subspaces defined by the singular vectors of attention heads. Turning to (Ahmad et al., 2025), the authors show that a single attention head “can simultaneously implement multiple, independent computations” that “can be activated or suppressed via interventions along individual directions in the SVD basis.” Next, the authors in (Pan et al., 2024) study the interaction between tokens (image patches) in vision transformers, and “propose that left and right singular vectors of the query-key interaction matrix can be seen as pairs of interacting feature directions,” thereby implicitly equating singular vectors with features. Finally, our paper builds most directly on (Franco & Crovella, 2024; 2025) which also relied on an assumption of SVF alignment in order to trace circuits, and introduced the notion of sparse attention decomposition, which we also use here (in Section 5).

Although each of the above studies relies on the alignment of SVF as a critical assumption, **no previous work has presented a detailed investigation of why and when SVF alignment occurs**. Finding initial answers to those questions is the goal of this paper.

Understanding why and when SVF alignment occurs is important. This is because when SVF alignment occurs, it offers a new strategy to attack a central problem in mechanistic interpretability: finding feature representations (Anwar et al., 2024; Sharkey et al., 2025). The question of how features are represented has driven a large body of work in mechanistic interpretability, with many studies showing that interpretable concepts in models are encoded in one-dimensional subspaces (Elhage et al., 2022; Olah et al., 2020; Mikolov et al., 2013; Alain & Bengio, 2018; Park et al., 2023; Gurnee & Tegmark, 2024; Gurnee et al., 2023; Marks et al., 2024) or in low-dimensional subspaces (Levy & Geva, 2025; Engels et al., 2025; Kantamneni & Tegmark, 2025; Hernandez et al., 2024). However, the strategies used to find feature representations to date all have drawbacks. The use of activation patching (Zhang & Nanda, 2024; Goldowsky-Dill et al., 2023; Wang et al., 2023; Conmy et al., 2023; Hanna et al., 2023; Lieberum et al., 2023) relies on carefully constructed counterfactuals and requires

multiple passes over the model, which is time consuming and error-prone, limiting scalability (Makelov et al., 2023; Mueller, 2024; McGrath et al., 2023; Rushing & Nanda, 2024). An alternative strategy uses Sparse Autoencoders (SAEs) (Huben et al., 2024; Bricken et al.), but these methods are expensive to train and have been shown to have significant drawbacks (Leask et al., 2025; Bushnaq; Gao et al., 2024; Bussmann et al.; Chanin et al., 2024); one reason for this may be that SAEs are built only from model activations and do not take into account model weights (bialchughtai & Bushnaq).

In contrast to methods like SAEs, exploiting SVF alignment uses the relationship between model activations *and* model weights. When SVF alignment holds, one can in principle consider the singular vectors of an attention head to be ‘candidate features’ and then examine activations to see if those features are present, as in (Franco & Crovella, 2024; 2025). In practice, feature identification using SVF alignment simply boils down to decomposing activations in the SVD basis – which can be done on a per-prompt basis and in a single forward pass over the model. Compared to the use of SAEs or linear probes, this offers a much more straightforward, efficient, and scalable approach; and, as we show in the body of this paper, it has theoretical and empirical justification.

3. Methods

We will generally be considering the setting in which a head is computing attention over a set of *key* tokens $S = \{s_i\}_{i=1}^m$. Token s_m is also the *query* token which we will denote as r .

Given a pair of tokens (r, s) for some $s \in S$, we will say that a head ‘attends to’ (r, s) when it computes a large attention value for (r, s) . There is no strict attention threshold that defines ‘attending’ to a token pair, but attention on the pair should at least be higher than the uniform distribution (i.e., $1/m$). As explained below, tokens are treated as sums of features. We assume that the head attends to a token pair because of the presence of certain features in the tokens. The set of features that can cause a head to attend to a token pair are the features ‘of interest’ to the head. We don’t assume that all features are of interest to any given head – many features, even if present, will not affect a head’s attention computation.

To explore the alignment of singular vectors with features, we use a toy model that allows both features and singular vectors to be directly observed. We start with the toy autoencoder model from (Elhage et al., 2022) defined over a universe of N features $\{w_i \in \mathbb{R}^D\}_{i=1}^N$. An input to the model f is a choice of *feature strengths*, constructed as $f_i = a_i b_i$ where $a_i \sim \text{Bernoulli}(p)$ and $b_i \sim U(0, 1)$. Internally, the model represents inputs as vectors in \mathbb{R}^D ;

we refer to the internal representations as tokens (using language model terminology). The model constructs a token as $r = Wf$ where $W \in \mathbb{R}^{D \times N}$ is the matrix whose columns are the features w_i . The autoencoder seeks to reconstruct f as $f' = \text{ReLU}(W^\top r + b)$ with $b \in \mathbb{R}^N$. The learned weights are W and b and the reconstruction loss is $\mathcal{L}_{\text{recon}} = \|f - f'\|_2^2$. In this model, ReLU and negative biases can eliminate some interference between representations, which lowers reconstruction loss. This model was extensively explored in (Elhage et al., 2022) and was shown to generate feature representations $\{w_i\}$ that ‘spread out’ to occupy the space \mathbb{R}^D approximately isotropically.

We extend this model to study the influence of the attention mechanism. We add an attention head that compares tokens r and s and generates an attention logit as $\ell = r^\top W_Q^\top W_K s$ for learned matrices $W_Q, W_K \in \mathbb{R}^{H \times D}$. W_Q and W_K always appear together, so as mentioned, we use Ω to denote $W_Q^\top W_K$. The head computes logits for a single query and multiple keys as $\ell_j(r, S) = r^\top \Omega s_j$, $j = 1, \dots, m$. The head then computes an output $p_{\text{head}} = \text{Softmax}(\ell_1, \dots, \ell_m)$.

To train the head, we assume that it should attend to a pair of tokens when specific pairs of features are present in the tokens. To allow for flexible experimentation, we parameterize the target at the logit level. For a pair of tokens (r, s) denote $f^{(r)}$ and $f^{(s)}$ as the corresponding feature strengths. For the token pair (r, s) we define the target logit as $\ell^T(r, s) = \sum_{ij} T_{ij} f_i^{(r)} f_j^{(s)}$. We then define $p_{\text{target}} = \text{Softmax}(\ell_1^T, \dots, \ell_m^T)$ over the m token pairs. This parameterization allows us to use T_{ij} to specify desired attention patterns in an intuitive fashion. We can interpret T_{ij} as the amount that should be added to the target logit to the extent features w_i and w_j are present in the corresponding tokens.

The training loss for the head is defined as $\mathcal{L}_{\text{attn}} = \text{Cross-Entropy}(p_{\text{head}}, p_{\text{target}})$. The overall loss for the model is $\mathcal{L} = \mathcal{L}_{\text{recon}} + \lambda \mathcal{L}_{\text{attn}}$. Details of the model and parameter sweeps showing robustness of results are provided in Appendix A.

Why this model? The idea that tokens are sums of features is consistent with much of the work in model interpretability. It is strongly supported by the residual-connection structure of the model as explained in (Elhage et al., 2021). It does not depend on the LRH but is fully consistent with the LRH. Similarly, much work in model interpretability assumes that heads attend to tokens because of the presence of specific features in those tokens. Hence the setting we describe here reflects only a minimal, commonly-adopted view of model internals. At the same time, our toy model allows for simultaneous learning of both feature representations (W) and model weights (Ω) and direct comparison of the two.

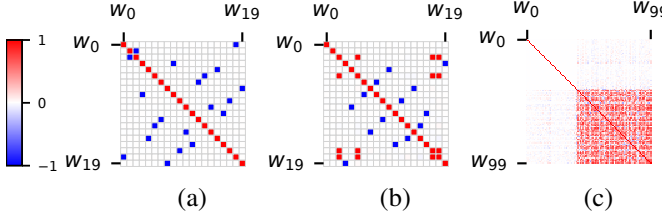


Figure 1. The geometry of features as illustrated via cosine similarities. (a) Without the attention head, features arrange isotropically. (b) With 20 features of which w_0, w_1 are of interest, features of interest orthogonalize against the others. (c) With 100 features in dimension 50, and 40 of those features are of interest (20 pairs), features of interest also orthogonalize against the others.

4. Singular Vectors Align with Features

To start, we examine a model incorporating $N = 20$ features, each represented in $D = 10$ dimensions; the head dimension is $H = 10$. As a warm-up we look at how features w_i (columns of W) arrange when the attention head is *not* included in the toy model. Cosine similarities among the features are shown in Figure 1(a). This setting is similar to the settings studied in (Elhage et al., 2022), and we see similar results: features arrange themselves into 10 pairs, one per dimension, with each pair antipodal. This arrangement is *isotropic* – features are spread equally in all directions. Formally, isotropy is the condition that WW^\top is a multiple of the identity (ie, W is a tight frame whose feature components are uncorrelated). As explained in (Elhage et al., 2022), this arrangement is expected as it minimizes *interference* – the reconstruction error caused by non-orthogonality of features. More details are in Appendix C (Figure 17).

Single-Feature-Pair Alignment. Next, we observe the effects of adding the attention head. We study the simplest possible case: the head attends to feature w_0 when present in the query token, and feature w_1 when present in the key token. To implement this we set $T_{01} = 1$, and $T_{ij} = 0$ elsewhere. We train the model, decompose the head’s weight matrix into its SVD $\Omega = U\Sigma V^\top$, and examine the alignment between features and singular vectors. Figure 2(a) shows that after training, **singular vectors are aligned with features**. Feature w_0 is aligned with left singular vector 0, and feature w_1 is aligned with right singular vector 0. The spectrum of Ω shows only a single large singular value, meaning that the head has allocated one of its dimensions entirely to representing and recognizing this feature pair.

Why does SVF alignment happen? Intuitively, the need for $w_0^\top \Omega w_1$ to output a relatively large value tends to align the vector Ωw_1 with w_0 . At the same time, the need for $w_i^\top \Omega w_1$ to output a smaller value for $i \neq 0$ means that Ωw_1 is less attracted to each of the other w_i s. The resulting tendency for Ωw_1 to be in the same direction as w_0 , and likewise $w_0^\top \Omega$ to be in the same direction as w_1 , means that $\Omega^\top \Omega w_1 \approx \alpha w_1$,

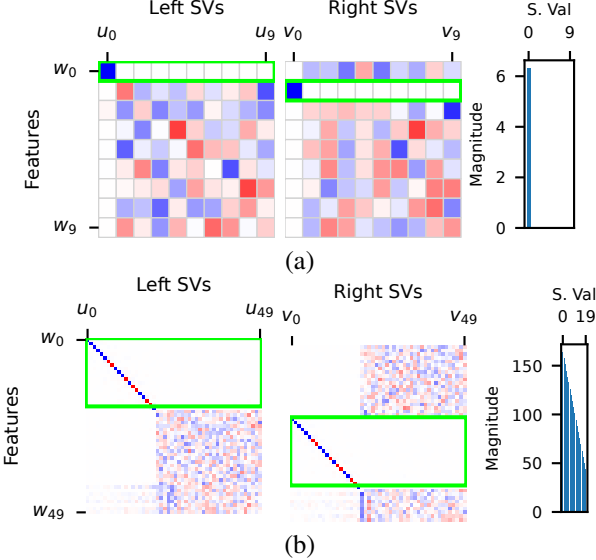


Figure 2. Singular vectors align with features (shown by green boxes). Cosine similarities of singular vectors and features, and magnitudes of singular values. (a) 20 Features of which w_0, w_1 are of interest; w_0 aligns only with u_0 and w_1 aligns only with v_0 . (b) 100 features of which $w_0 \dots w_{39}$ are of interest. For clarity, only an initial subset of features is shown; full figures are in Appendix A.

ie, w_1 is approximately a right singular vector of Ω . An analogous argument establishes that w_0 is approximately a left singular vector of Ω .

SVF alignment *provably* occurs under fairly general conditions. In Appendix B.2 we present theorems characterizing example conditions under which SVF alignment is guaranteed. We consider a setting in which features (W) are fixed, and the head’s weights (Ω) are allowed to vary. First, we show in Theorem 2 that if features are in isotropic position, and a single pair of features are of interest to the head, then after training the top singular vectors of Ω will be exactly aligned with the attended features. Second, we show in Theorem 3 that even when features deviate from isotropy, singular vector alignment occurs approximately whenever the interference (inner products) between the features is sufficiently bounded. Note that, as discussed above, interference between features will typically be low so as to keep the model’s reconstruction error low.

Turning to the geometry of features, Figure 1(b) shows a second effect. Features w_0 and w_1 are orthogonal to *all other features*. This is not necessary for alignment per se, and deserves investigation. Intuitively, the remaining features have shifted into the $D - 2$ dimensional subspace that is orthogonal to the span of $\{w_0, w_1\}$.

We hypothesize that orthogonalization occurs to minimize reconstruction loss. This is provably the case for a model like ours. Theorem 4 in Appendix B.3 considers the case in

which Ω is fixed while features are allowed to vary. It shows that in a setting where there is a penalty for interference among features (as in our toy model), the solution found to the training objective of the model will be the one in which features are orthogonal.

Multi-Feature-Pair Alignment. SVF alignment extends to cases involving multiple feature pairs. We observe that when multiple feature pairs are of interest to the head,² all features are typically still aligned with singular vectors. As an example, we show a model run with 100 features and hidden dimension 50. We set the target logits for feature pairs as $T_{i,i+20} = 26 - i$ for $0 \leq i < 20$ (zero otherwise). This causes 20 feature pairs $(i, i + 20)$ to be attended by the head, with logit values linearly declining in i . Figure 2(b) shows that all features align with singular vectors, and that the singular values of the head reflect the values of the target logits.

We attribute the phenomenon of alignment in the multi-feature case to the interaction of the two effects: alignment of the top singular vectors to most important features, and the resulting orthogonalization of the remaining features. Figure 1(c) shows the geometric arrangement of features in this case, confirming orthogonalization of the remaining features. We hypothesize that during training, singular vectors align with features to minimize attention loss, while at the same time features orthogonalize to minimize reconstruction loss. Because singular vectors can shift during training, features can orthogonalize without impacting attention loss.

Evidence for this hypothetical mechanism comes from observation of the evolution of features and singular vectors during training. We use as an example a model run with 20 features and 10 hidden dimensions. We again set linearly declining target logits, in this case for only four pairs of features $(i, i + 4)$ for $i = 0, 1, 2, 3$. We confirm at the end of 10,000 training steps that features have aligned with singular vectors.

The dynamics of SVF alignment during training are shown in Figure 3, which shows similarity between vectors at different time steps. Singular vectors align with features individually over time, in order of their impact on attention loss. Consistent with our hypothesis, we see that both singular vectors and features evolve over time. Additionally, comparing each feature’s evolution with the corresponding singular vector, it appears that singular vectors tend to shift first, after which features shift so as to align with their corresponding singular vector.

The results shown here are robust over a wide range of model parameters. In Appendix A we show that SVF alignment

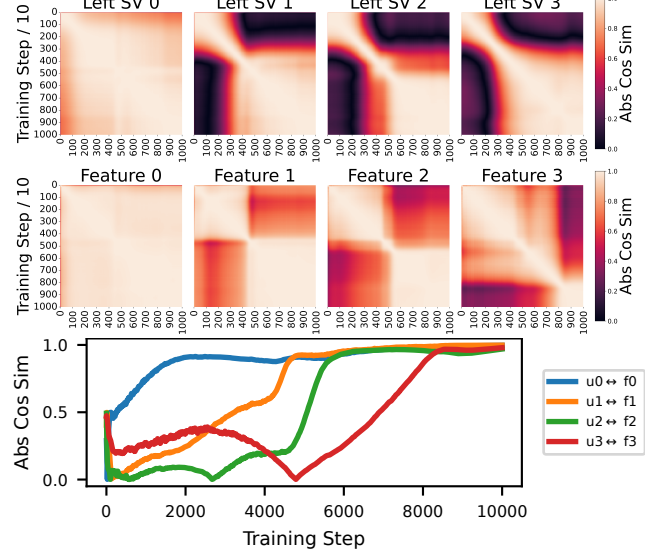


Figure 3. Both singular vectors and features evolve during training, and alignment occurs for highest-logit features first. Above: Cosine similarities showing evolution of singular vectors (top) and features (bottom). Below: Cosine similarities showing evolution of alignment of singular vectors with features.

arises consistently over variations in relative loss weight λ , number of features N , context length m , head dimension H , and across random seeds.

Finally, we note that we have so far studied the setting in which the number of features of interest to the head is less than the head capacity H . We believe that studying this regime is itself important, and can provide a foundation for follow-on studies of the regime in which there are more features of interest than head dimensions. In Appendix D we use the toy model to probe the latter regime, noting that some features move into superposition within the head’s representation space – but for the majority of singular vectors, SVF alignment still holds.

Results: Toy Model

- The presence of an attention head causes singular vectors to align with features.
- Multiple features will align with corresponding singular vectors, up to the dimension of the head.
- Both features and singular vectors evolve during training to come into alignment.

5. Sparse Attention Decomposition

The preceding sections provide theoretical and empirical support for the hypothesis that under some conditions, the singular vectors of an attention head will be aligned with features of interest to the head. The next question is: **does**

²For a number of features up to the head dimension; we discuss below.

SVF alignment happen in real models? This is important, because if it does happen, then by examining singular vectors in a model we may be able to identify actual features being used by that model. In fact, this assumption was implicit in the strategies taken in (Merullo et al., 2024; Ahmad et al., 2025; Pan et al., 2024; Franco & Crovella, 2024; 2025).

In a real model, we cannot conclusively establish that a singular vector is aligned with a particular feature without *a priori* knowledge of that feature’s representation in the model. However, the hypothesis that singular vectors and features are aligned does lead to predictions that are testable in a real model. We focus on one prediction: *sparse attention decomposition* (Franco & Crovella, 2024; 2025). We first analyze logits to build intuition, and then we extend the analysis to attention.

Analyzing Logits. To illustrate, let’s suppose features are aligned with singular vectors, either exactly (as in Theorem 2 or Figure 2) or approximately (as in Theorem 3). Further, features that are not of interest are (approximately) orthogonal to features that are of interest, as in Figures 1(b) or 1(c) or Theorem 4. We’ll term this set of assumptions the *alignment hypothesis*.

Now consider a head’s logit decomposed in the singular vectors of Ω :

$$\begin{aligned} \ell(r, s) = r^\top \Omega s &= \sum_k r^\top u_k \sigma_k v_k^\top s & (1) \\ &= \sum_k \sum_{i,j} f_i^{(r)} \underbrace{w_i^\top u_k}_{\sigma_k} \underbrace{v_k^\top w_j}_{f_j^{(s)}} & (2) \end{aligned}$$

The bracketed terms show that we can think of the attention head as ‘testing’ each feature against each singular vector, and outputting a large value only when two features match a common pair of singular vectors (ie, having the same k). Under the alignment hypothesis, an individual term (k, i, j) in (2) will only be large if features i and j are present, and aligned with singular vectors k . Now, in a real model we cannot in general observe the terms in (2) – however, we *can* observe the terms in (1). Because terms in (2) will only be large for singular vectors (values of k) aligned with features present in the tokens, the same is true of (1). In other words, when a head assigns a large logit ℓ to a pair of tokens because they contain a specific, limited set of features, the logit decomposed in the SVD basis can show a sparse representation.³

Sparse attention decomposition provides a powerful tool for interpretability, for two reasons. First, the presence of a few large terms in (1) suggest that the corresponding singular vectors may encode *representations* of features. And second,

³The observed sparsity is *not* attributable simply to the attention matrix being low-rank or ill-conditioned, as we discuss below.

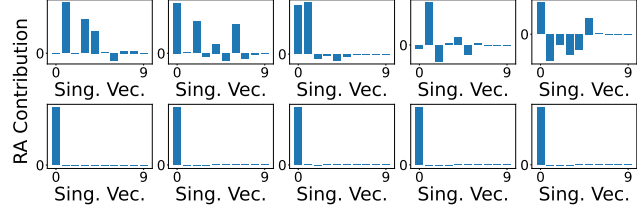


Figure 4. Relative attention decomposition is sparse when a single feature pair is present. Top: Early in training; Bottom: Late in training.

if attention is sparsely decomposed in the SVD basis, then only a small set of dimensions in the tokens contain features important for the attention computation. This ‘reduces the search space’ of causal features, a concept that is important in (Merullo et al., 2024; Franco & Crovella, 2024; 2025).

Extending to Attention. Next we consider how computing attention via Softmax affects sparse attention decomposition. Placing attention on a token pair requires putting a higher logit on the attended token than on the other key tokens. Hence when a model attends to (r, s_j) , the alignment hypothesis would predict not that $\ell(r, s_j)$ *per se* is sparse in the SVD basis, but rather that $\ell(r, s_j) - \ell(r, s_i)$, $j \neq i$, is sparse in the SVD basis.

To extend this observation to an arbitrary context length m , we use the notion of *relative attention* (Franco & Crovella, 2025). Over a set of logits $\ell_j(r, S)_{j=1}^m$, relative attention on token j is defined as $\tilde{\ell}_j = \ell_j - \frac{1}{m-1} \sum_{i \neq j} \ell_i$. As shown in (Franco & Crovella, 2025) this metric has the useful property that if attention on (r, s_j) is greater than $1/m$ (the uniform distribution) then $\tilde{\ell}_j > 0$. To decompose relative attention we can simply apply (1) with $s = s_j - \frac{1}{m-1} \sum_{i \neq j} s_i$.

Evidence in the Toy Model. First, we show that sparse attention decomposition emerges during training. We illustrate using the model run from Figure 3 in which there are four feature pairs of interest to the head. Figure 4 shows the decomposition of relative attention for inputs where feature pair $(0, 4)$ are the only features of interest present, both early and late in training. At first, relative attention does not show sparse decomposition, but later on the single feature of interest results in only one significant contribution to relative attention. In Appendix E we show additional examples (Figure 19) showing that sparsity does *not* emerge when features of interest are *not* present.

As Figure 4 suggests, a contribution from a particular singular vector pair is indicative of the presence of a corresponding feature pair in the inputs. In Figure 5 we show further confirmation of this effect. The figure shows that the strength of contribution to relative attention correlates with feature strength in the input. This supports the use of SVF

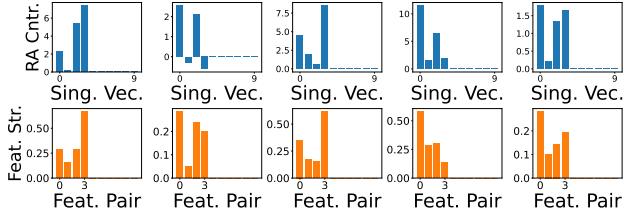


Figure 5. Sparse attention decomposition identifies feature presence. Top: Decomposition of relative attention across all 10 singular vectors for five token pairs (r, s) . Bottom: Feature strength $(f_i^{(r)} f_{i+4}^{(s)})$ for the four corresponding feature pairs w_i, w_{i+4} .

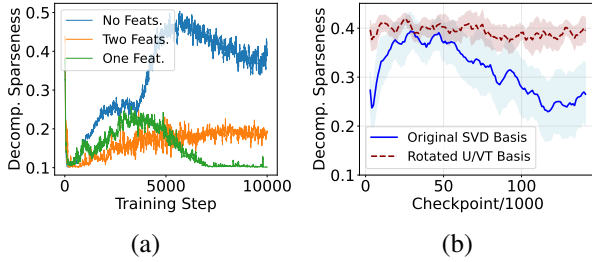


Figure 6. Sparse attention decomposition emerges during training: $S(v)$ metric, smaller is sparser, shaded regions are 95% confidence intervals. (a) Toy Model (b) Pythia-160M, for the IOI attention heads and token pairs identified in (Tigges et al., 2024). Sparsity is not due to attention matrices being low-rank, as shown by the comparison to spectrum-preserving rotations of the SVD bases.

alignment as a means of identifying the features of interest that are present in a token pair.

We show emergence of sparsity quantitatively using the metric from (Rolls & Tovee, 1995): $S(v) = (\frac{1}{n} \sum_i |v_i|)^2 / \frac{1}{n} \sum_i v_i^2$. This metric takes on a value of 1 when inputs are minimally sparse (all equal), and a value of $1/n$ when inputs are maximally sparse (only one nonzero value). For any given head and token pair, we compute $S(v)$ over the decomposition of relative attention.

Figure 6(a) shows how sparsity emerges in the toy model. We consider three classes of token pairs: pairs where only one feature of interest is present, pairs where two are present, and pairs where no features of interest are present; we measure decomposition sparsity using the $S(v)$ metric. The figure shows that when features of interest are present, attention decomposition is sparse, and it is sparser when fewer features are present. On the other hand, when features of interest are absent, attention decomposition is much less sparse. The dynamics are consistent with the evolution of SVF alignment seen in Figure 3, supporting the notion that as singular vectors align with features, attention decomposition becomes sparse.

Evidence in Language Models. As discussed, sparse attention decomposition is a prediction of SVF alignment that

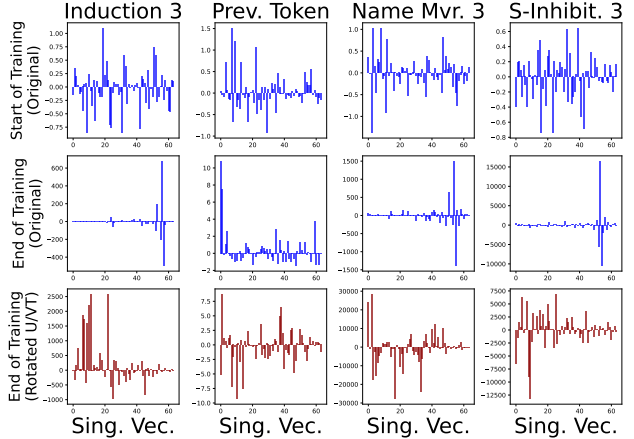


Figure 7. Sparse attention decomposition emerges after training in Pythia. Top: Early in training; Middle: Late in training. Bottom: Sparse decomposition does not arise with randomly rotated singular vectors. Note that singular vectors are ordered by decreasing singular value, showing that often the largest contributors to relative attention come from among the *smallest* singular values.

is testable in real language models. We start with Pythia-160M (Biderman et al., 2023), which provides 130 checkpoints taken at intervals of 1000 training epochs. We input to the model a prompt from the Indirect Object Identification (IOI) task, and we capture relative attention at the heads and token pairs previously identified as part of the IOI circuit (Tigges et al., 2024). Further details are in Appendix F.

Figure 7 shows the decomposition of relative attention for four attention heads, at the start and end of training. In each case, relative attention decomposition becomes significantly sparse, with most of the contribution to relative attention coming from a small set of singular vectors of the attention head. Not all attention heads show such strong sparsity emergence (we present all head decompositions in Appendix F), which may be due to a larger number of features playing a role in some attention heads.

Quantitatively, attention sparsity emerges in Pythia in a manner similar to the dynamics of the toy model. Figure 6(b) shows the evolution of the $S(v)$ metric during training of Pythia. Here, $S(v)$ is averaged over all heads in the IOI circuit, and the general shape of sparsity emergence is similar to the single-feature case for the toy model.

Sparse attention decomposition is *not* attributable simply to low-rank properties of attention matrices. First, Figure 7 (middle) shows that the largest terms in (1) can be those with the *smallest* singular values, which is the opposite of what would be expected if low-rank properties were the cause. More directly, we show that sparse decomposition is not a result of low-rank properties by recomputing $S(v)$ after randomly rotating the U and V singular vector matrices. This modification reorients singular vectors *without* changing the

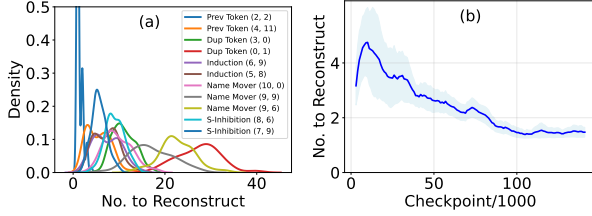


Figure 8. No. of singular vectors to reconstruct relative attention. (a) GPT-2, after training; (b) Pythia, during training, 95% CI.

matrix spectrum or rank. Figure 6(b) shows that the decline in $S(v)$ disappears when the SVD basis is randomly rotated, showing that the observed sparsity is due to the specific alignment of certain directions with certain singular vectors. Figure 7 (bottom) shows visually the absence of sparsity under rotated U and V .

As suggested by Figure 5, the contributions made by singular vectors to relative attention can indicate the presence of features of interest in the input. As a measure of the potential number of features of interest present in a token pair, we define $N_{\text{recon}}(j)$ to count the minimum number of singular vectors needed to ‘reconstruct’ relative attention on key token s_j .⁴ This metric separates the relative attention contributions of singular vectors into ‘signal’ and ‘noise.’

Using N_{recon} we can estimate how many features of interest may be present when an attention head attends to a token pair. Figure 8(b) shows how this metric changes over the duration of training in Pythia. It shows that for the heads considered here, typically only 1-4 singular vectors are needed to reconstruct relative attention and shows how this value declines during training (consistent with Figure 6(b)).

As further confirmation of sparse attention decomposition, we examine the N_{recon} metric for GPT-2 on the IOI task (Wang et al., 2023). Figure 8(a) shows distributions of the reconstruction count for different attention heads of the trained model. Typical values vary reflecting different functional roles of the attention heads, but they show that in most cases, N_{recon} is small, showing that features of interest occupy low-dimensional subspaces, and suggesting that only a limited number of features are of interest to each head.

Results: Sparse Attention Decomposition (SAD)

- Under SVF alignment, if a limited number of features of interest are present, attention will decompose sparsely in the SVD basis (SAD).
- In both toy and real models, we see SAD.
- In real models, SAD evolves during training in a manner consistent with the toy model.

⁴Specifically, $N_{\text{recon}}(j)$ is the size of the smallest set of terms in (1) whose sum equals or exceeds the relative attention on key token s_j .

6. Discussion

Limitations. In this paper, directly examining features in real models is out of scope. However, a number of studies have shown in real models that features derived from SVF alignment are interpretable (Ahmad et al., 2025; Pan et al., 2024; Franco & Crovella, 2024) and causal for model performance (Franco & Crovella, 2025). Hence our focus here has instead been on clearly establishing the underlying theoretical and empirical evidence for SVF alignment.

While the evidence shows that singular vectors align closely with features in the toy model, it is possible that in real models at least some singular vectors align with ‘cone directions’ (directions that are overrepresented among features) due to anisotropy (Godey et al., 2024; Li et al., 2025). The fact that singular-vector derived features are often interpretable (Ahmad et al., 2025; Pan et al., 2024; Franco & Crovella, 2024) suggests, at minimum, that many singular vectors are *not* influenced by ‘cone directions,’ but more work is needed to understand the importance of feature anisotropy.

While our results shed light on why and when the singular vectors of attention heads align with features, we only scratch the surface of the phenomenon. For example, there are questions related to the *number* of features that are of interest to head. When there are more features of interest to a head than the head has dimensions to represent (H in our model), how are features deconflicted? We present some evidence in Appendix D that the least ‘important’ features will share a common singular vector pair, but more work is needed, both experimentally and theoretically, to understand what can happen in general. Second, our work is limited to the study of a single head. Across the multiple heads in a real model, how are singular vectors in aggregate allocated among features? Note that there is evidence that an important benefit of multi-head attention is the ability to deconflict features, ie, to suppress noise in the attention mechanism arising from feature interference (Adler, 2025). Further, there is evidence that some singular vectors are nearly identical across multiple heads (the so-called ‘control signals’ in (Franco & Crovella, 2025)). Third, is there a higher level at which to view the set of singular vectors in use across all heads in a model? The authors in (Jermyn et al.) show a toy-model case in which multiple heads work in superposition to compute a single output. Can we observe coordinated use of singular vectors across multiple heads?

Conclusion

Despite the number of open questions our study leaves, our results show that SVF alignment has strong empirical and theoretical justification. As such, it has potential as a valuable tool for feature identification in language models.

Acknowledgments

This work benefited from early feedback from Aaron Mueller and Micah Adler. The authors gratefully acknowledge consultations with ChatGPT in developing the theorems and Claude Code in developing the experiments. This research was funded by a grant from Coefficient Giving and by NSF award CNS-2312711.

Impact Statement

This paper presents work whose goal is to advance the field of Machine Learning. There are many potential societal consequences of our work, none which we feel must be specifically highlighted here.

References

Adler, M. On the capacity of self-attention, 2025. URL <https://arxiv.org/abs/2509.22840>.

Ahmad, A., Joshi, A., and Modi, A. Beyond components: Singular vector-based interpretability of transformer circuits. In *Proceedings of NeurIPS*, 2025.

Alain, G. and Bengio, Y. Understanding intermediate layers using linear classifier probes, 2018. URL <https://arxiv.org/abs/1610.01644>.

Anwar, U., Saparov, A., Rando, J., Paleka, D., Turpin, M., Hase, P., Lubana, E. S., Jenner, E., Casper, S., Sourbut, O., Edelman, B. L., Zhang, Z., Günther, M., Korinek, A., Hernandez-Orallo, J., Hammond, L., Bigelow, E., Pan, A., Langosco, L., Korbak, T., Zhang, H., Zhong, R., Ó hÉigearaigh, S., Recchia, G., Corsi, G., Chan, A., Anderljung, M., Edwards, L., Petrov, A., de Witt, C. S., Motwan, S. R., Bengio, Y., Chen, D., Torr, P. H. S., Albanie, S., Maharaj, T., Foerster, J., Tramer, F., He, H., Kasirzadeh, A., Choi, Y., and Krueger, D. Foundational challenges in assuring alignment and safety of Large Language Models, 2024. URL <https://arxiv.org/abs/2404.09932>.

Biderman, S., Schoelkopf, H., Anthony, Q. G., Bradley, H., O'Brien, K., Hallahan, E., Khan, M. A., Purohit, S., Prashanth, U. S., Raff, E., et al. Pythia: A suite for analyzing large language models across training and scaling. In *International Conference on Machine Learning*, pp. 2397–2430. PMLR, 2023.

bilalchughtai and Bushnaq, L. Activation space interpretability may be doomed. <https://www.lesswrong.com/posts/gYfpPbww3wQRaxAFD/activation-space-interpretability-may-be-doomed>.

Bricken, T., Templeton, A., Batson, J., Chen, B., Jermyn, A., Conerly, T., Turner, N. L., Anil, C., Denison, C., Askell, A., Lasenby, R., Wu, Y., Kravec, S., Schiefer, N., Maxwell, T., Joseph, N., Tamkin, A., Nguyen, K., McLean, B., Burke, J. E., Hume, T., Carter, S., Henighan, T., and Olah, C. Towards monosemanticity: Decomposing language models with dictionary learning. <https://transformer-circuits.pub/2023/monosemantic-features>.

Bushnaq, L. Lesswrong post. <https://www.lesswrong.com/posts/cCgxp3Bq4aS9z5xqd/lucius-bushnaq-s-shortform?commentId=wETE2ebypKzAdH8De>.

Bussmann, B., Pearce, M., Leask, P., Bloom, J., Sharkey, L., and Nanda, N. Showing SAE latents are not atomic using Meta-SAEs. <https://www.lesswrong.com/posts/TMAMh4DdMr4nCSr5/showing-sae-latents-are-not-atomic-using-meta-saes>.

Chanin, D., Wilken-Smith, J., Dulka, T., Bhatnagar, H., and Bloom, J. A is for absorption: Studying feature splitting and absorption in sparse autoencoders, 2024. URL <https://arxiv.org/abs/2409.14507>.

Conmy, A., Mavor-Parker, A., Lynch, A., Heimersheim, S., and Garriga-Alonso, A. Towards automated circuit discovery for mechanistic interpretability. In Oh, A., Naumann, T., Globerson, A., Saenko, K., Hardt, M., and Levine, S. (eds.), *Advances in Neural Information Processing Systems*, volume 36, pp. 16318–16352. Curran Associates, Inc., 2023. URL https://proceedings.neurips.cc/paper_files/paper/2023/file/34e1dbe95d34d7ebaf99b9bcaeb5b2be-Paper-Conference.pdf.

Elhage, N., Nanda, N., Olsson, C., Henighan, T., Joseph, N., Mann, B., Askell, A., Bai, Y., Chen, A., Conerly, T., DasSarma, N., Drain, D., Ganguli, D., Hatfield-Dodds, Z., Hernandez, D., Jones, A., Kernion, J., Lovitt, L., Ndousse, K., Amodei, D., Brown, T., Clark, J., Kaplan, J., McCandlish, S., and Olah, C. A Mathematical Framework for Transformer Circuits. *Transformer Circuits Thread*, 2021. URL <https://transformer-circuits.pub/2021/framework/index.html>.

Elhage, N., Hume, T., Olsson, C., Schiefer, N., Henighan, T., Kravec, S., Hatfield-Dodds, Z., Lasenby, R., Drain, D., Chen, C., Grosse, R., McCandlish, S., Kaplan, J., Amodei, D., Wattenberg, M., and Olah, C. Toy Models of Superposition. *Transformer Circuits Thread*, 2022. URL https://transformer-circuits.pub/2022/toy_model/.

Engels, J., Michaud, E. J., Liao, I., Gurnee, W., and Tegmark, M. Not all language model features are one-dimensionally linear, 2025. URL <https://arxiv.org/abs/2405.14860>.

Franco, G. and Crovella, M. Sparse attention decomposition applied to circuit tracing. Technical Report 2410.00340, 2024. URL <https://arxiv.org/abs/2410.00340>.

Franco, G. and Crovella, M. Pinpointing attention-causal communication in language models. In *Proceedings of NeurIPS*, San Diego, CA, 2025. doi: TBD. URL [TBD](#).

Gao, L., la Tour, T. D., Tillman, H., Goh, G., Troll, R., Radford, A., Sutskever, I., Leike, J., and Wu, J. Scaling and evaluating sparse autoencoders, 2024. URL <https://arxiv.org/abs/2406.04093>.

Godey, N., Clergerie, É., and Sagot, B. Anisotropy is inherent to self-attention in transformers. In Graham, Y. and Purver, M. (eds.), *Proceedings of the 18th Conference of the European Chapter of the Association for Computational Linguistics (Volume 1: Long Papers)*, pp. 35–48, St. Julian’s, Malta, March 2024. Association for Computational Linguistics. doi: 10.18653/v1/2024.eacl-long.3. URL <https://aclanthology.org/2024.eacl-long.3/>.

Goldowsky-Dill, N., MacLeod, C., Sato, L., and Arora, A. Localizing model behavior with path patching, 2023. URL <https://arxiv.org/abs/2304.05969>.

Gurnee, W. and Tegmark, M. Language models represent space and time. In *The Twelfth International Conference on Learning Representations, ICLR 2024, Vienna, Austria, May 7-11, 2024*. OpenReview.net, 2024. URL <https://openreview.net/forum?id=jE8xbmvFin>.

Gurnee, W., Nanda, N., Pauly, M., Harvey, K., Troitskii, D., and Bertsimas, D. Finding neurons in a haystack: Case studies with sparse probing. *arXiv*, 2023. doi: 10.48550/arxiv.2305.01610.

Hanna, M., Liu, O., and Variengien, A. How does gpt-2 compute greater-than?: Interpreting mathematical abilities in a pre-trained language model. *arXiv*, 2023. doi: 10.48550/arxiv.2305.00586.

Hernandez, E., Sharma, A. S., Haklay, T., Meng, K., Wattenberg, M., Andreas, J., Belinkov, Y., and Bau, D. Linearity of relation decoding in transformer language models, 2024. URL <https://arxiv.org/abs/2308.09124>.

Horn, R. A. and Johnson, C. R. *Matrix Analysis*. Cambridge University Press, 2 edition, 2012.

Huben, R., Cunningham, H., Smith, L. R., Ewart, A., and Sharkey, L. Sparse autoencoders find highly interpretable features in language models. In *The Twelfth International Conference on Learning Representations*, 2024. URL <https://openreview.net/forum?id=F76bwRSLeK>.

Jermyn, A., Olah, C., and Henighan, T. Attention head superposition. <https://transformer-circuits.pub/2023/may-update/index.html#attention-superposition>.

Kantamneni, S. and Tegmark, M. Language models use trigonometry to do addition, 2025. URL <https://arxiv.org/abs/2502.00873>.

Leask, P., Bussmann, B., Pearce, M., Bloom, J., Tigges, C., Moubayed, N. A., Sharkey, L., and Nanda, N. Sparse autoencoders do not find canonical units of analysis, 2025. URL <https://arxiv.org/abs/2502.04878>.

Levy, A. A. and Geva, M. Language models encode numbers using digit representations in base 10, 2025. URL <https://arxiv.org/abs/2410.11781>.

Li, Y., Michaud, E. J., Baek, D. D., Engels, J., Sun, X., and Tegmark, M. The geometry of concepts: Sparse autoencoder feature structure. *Entropy*, 27(4), 2025. ISSN 1099-4300. doi: 10.3390/e27040344. URL <https://www.mdpi.com/1099-4300/27/4/344>.

Lieberum, T., Rahtz, M., Kramár, J., Nanda, N., Irving, G., Shah, R., and Mikulik, V. Does circuit analysis interpretability scale? evidence from multiple choice capabilities in chinchilla. *arXiv*, 2023. doi: 10.48550/arxiv.2307.09458.

Makelov, A., Lange, G., and Nanda, N. Is this the subspace you are looking for? an interpretability illusion for subspace activation patching. *arXiv*, 2023. doi: 10.48550/arxiv.2311.17030.

Marks, S., Rager, C., Michaud, E. J., Belinkov, Y., Bau, D., and Mueller, A. Sparse feature circuits: Discovering and editing interpretable causal graphs in language models. *arXiv*, 2024.

McGrath, T., Rahtz, M., Kramar, J., Mikulik, V., and Legg, S. The hydra effect: Emergent self-repair in language model computations. *arXiv*, 2023. doi: 10.48550/arxiv.2307.15771.

Merullo, J., Eickhoff, C., and Pavlick, E. Talking heads: Understanding inter-layer communication in transformer language models. In *Proceedings of NeurIPS*, 2024.

Mikolov, T., Yih, W.-t., and Zweig, G. Linguistic regularities in continuous space word representations. In Vanderwende, L., Daumé III, H., and Kirchhoff, K. (eds.), *Proceedings of the 2013 Conference of the North American Chapter of the Association for Computational Linguistics: Human Language Technologies*, pp. 746–751, Atlanta, Georgia, June 2013. Association for Computational Linguistics. URL <https://aclanthology.org/N13-1090>.

Mueller, A. Missed causes and ambiguous effects: Counterfactuals pose challenges for interpreting neural networks. *arXiv*, 2024. doi: 10.48550/arxiv.2407.04690.

Olah, C., Cammarata, N., Schubert, L., Goh, G., Petrov, M., and Carter, S. Zoom in: An introduction to circuits. *Distill*, 5(3):e00024–001, 2020.

P.-Å. Wedin. Perturbation bounds in connection with singular value decomposition. *BIT Numerical Mathematics*, 1972. URL <https://link.springer.com/article/10.1007/BF01932678>.

Pan, X., Philip, A., Xie, Z., and Schwartz, O. Dissecting query-key interaction in vision transformers. In *Proceedings of NeurIPS*, 2024.

Park, K., Choe, Y. J., and Veitch, V. The linear representation hypothesis and the geometry of large language models. In *Causal Representation Learning Workshop at NeurIPS 2023*, 2023. URL <https://openreview.net/forum?id=T0Po0Jg8cK>.

Rolls, E. T. and Tovee, M. J. Sparseness of the neuronal representation of stimuli in the primate temporal visual cortex. *Journal of Neurophysiology*, 73(2):713–726, 1995. ISSN 0022-3077. doi: 10.1152/jn.1995.73.2.713.

Rushing, C. and Nanda, N. Explorations of self-repair in language models. *arXiv*, 2024. doi: 10.48550/arxiv.2402.15390.

Sharkey, L., Chughtai, B., Batson, J., Lindsey, J., Wu, J., Bushnaq, L., Goldowsky-Dill, N., Heimersheim, S., Ortega, A., Bloom, J., Biderman, S., Garriga-Alonso, A., Conmy, A., Nanda, N., Rumbelow, J., Wattenberg, M., Schoots, N., Miller, J., Michaud, E. J., Casper, S., Tegmark, M., Saunders, W., Bau, D., Todd, E., Geiger, A., Geva, M., Hoogland, J., Murfet, D., and McGrath, T. Open problems in mechanistic interpretability, 2025. URL <https://arxiv.org/abs/2501.16496>.

Tigges, C., Hanna, M., Yu, Q., and Biderman, S. LLM circuit analyses are consistent across training and scale. In *The Thirty-eighth Annual Conference on Neural Information Processing Systems*, 2024. URL <https://openreview.net/forum?id=3Ds5vNudIE>.

Wang, K. R., Variengien, A., Conmy, A., Shlegeris, B., and Steinhardt, J. Interpretability in the wild: a circuit for indirect object identification in GPT-2 small. In *The Eleventh International Conference on Learning Representations, ICLR 2023, Kigali, Rwanda, May 1-5, 2023*. OpenReview.net, 2023. URL <https://openreview.net/forum?id=NpsVSN6o4ul>.

Zhang, F. and Nanda, N. Towards best practices of activation patching in language models: Metrics and methods, 2024. URL <https://arxiv.org/abs/2309.16042>.

A. Robustness of SVF Alignment in Toy Model

A.1. Toy Model Details

As described in the body of the paper, our model builds on the toy model used in (Elhage et al., 2022). We add to that model an attention head as described in Section 3.

The model is optimized using AdamW. Learning rate begins at 1e-3, and follows a cosine decay. The model uses a batch size of 1,024 key tokens, and 1,024 / m query tokens. We train until results stabilize, which takes between 10,000 and 80,000 steps depending on the configuration.

Full Alignment Plots Here we show complete plots of the alignment of singular vectors with features for the two cases we discuss in Section 4. Figure 9 shows that singular vectors align with features in both cases.

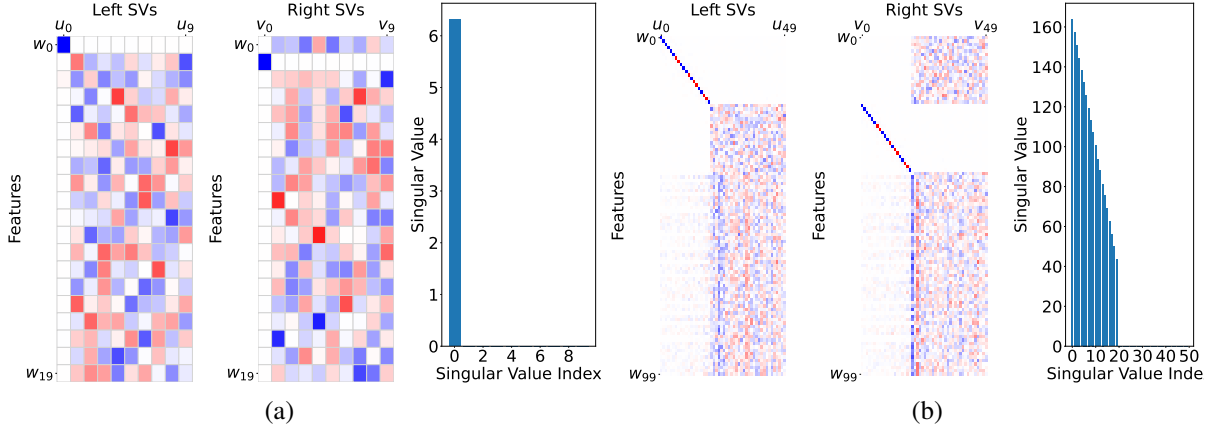


Figure 9. Singular vectors align with features. For $\Omega = U\Sigma V^\top$, cosine similarities of W and U , W and V , and spectrum (diagonal of Σ). This is an expanded view of Figure 2. (a) 20 Features of which w_0, w_1 are of interest; w_0 aligns with u_0 and w_1 aligns with v_0 . (b) 100 Features of which $w_0 \dots w_{39}$ are of interest. Due to sign ambiguities in SVD, SVF alignment yields cosine similarities that are either both positive or both negative.

A.2. Robustness

Here we show that SVF alignment arises robustly across a wide range of model parameters. We show this by starting from a default model configuration and varying various aspects of the model. The default configuration is shown in Table 1.

N	Number of features	20
D	Token dimension	10
H	Head dimension	10
λ	Weight of $\mathcal{L}_{\text{attn}}$ in loss	4
m	Context length	4
p	Feature probability	0.52

Table 1. Default Model Settings for Parameter Sweeps

Throughout this section, we study the case in which four feature pairs are of interest. Feature pair (0, 4) has target logit of 24, feature pair (1, 5) has target logit of 21, feature pair (2, 6) has target logit of 18, and feature pair (3, 7) has target logit of 15. These values are chosen to provide sufficient difference in attention after application of Softmax. As discussed in Section 4, the feature pair having the largest logit will generally map to the first singular vector, etc. To demonstrate SVF alignment we report the absolute cosine similarity between a feature and the singular vector that it corresponds to, in light of this mapping.

Feature Probability. As described in Section 3, features are present in the token with probability p . We study feature probabilities from 1 down to 0.02 in exponentially declining steps. Note that for feature probabilities greater than 0.05 in the default case, the token will in expectation be the sum of multiple features. Thus for most cases we study, the attention head does not ‘see’ any features themselves; features are mixed together in a token.

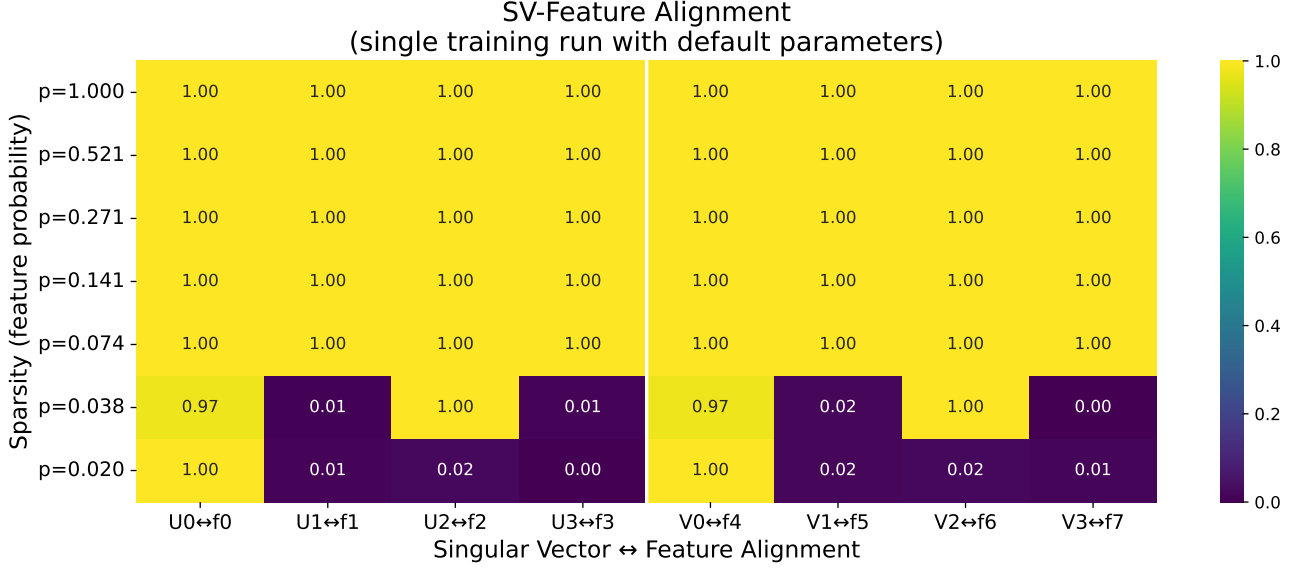


Figure 10. SVF Alignment is robust to feature probability.

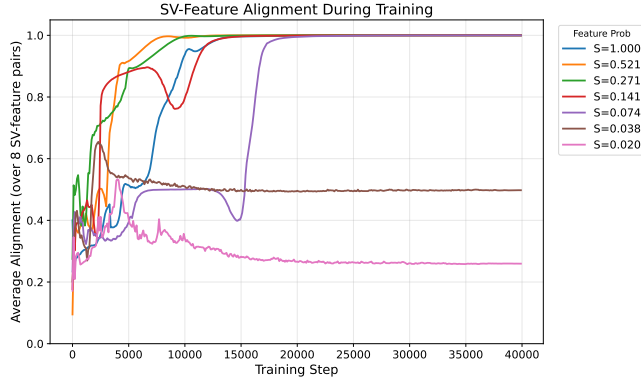


Figure 11. SVF Alignment arises earlier when features occur more frequently

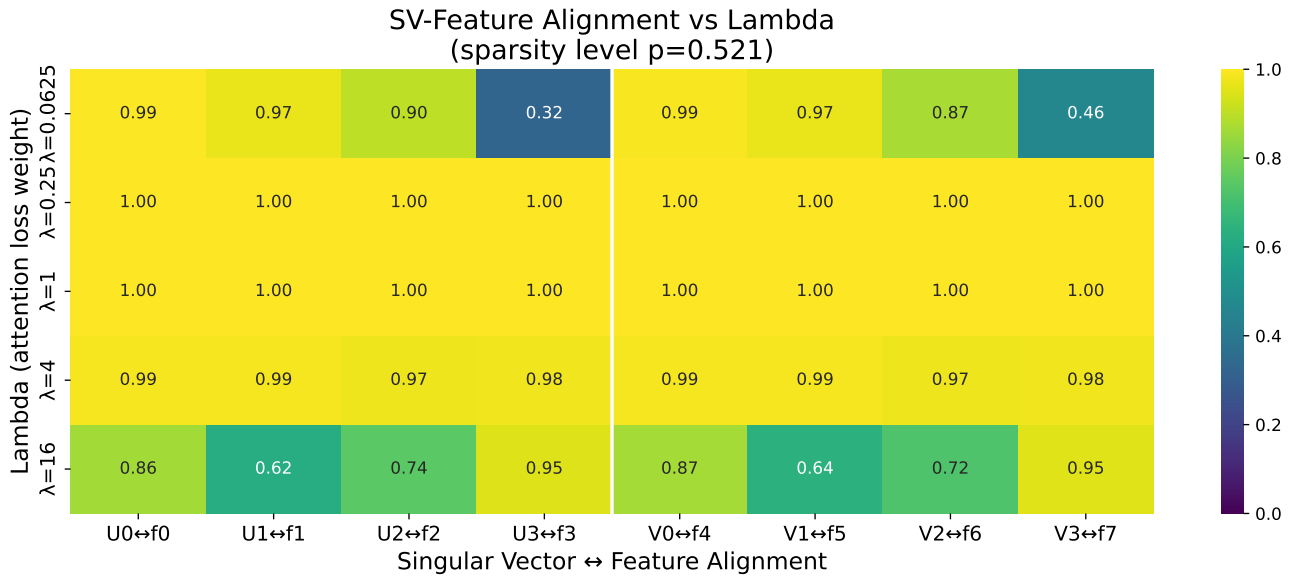
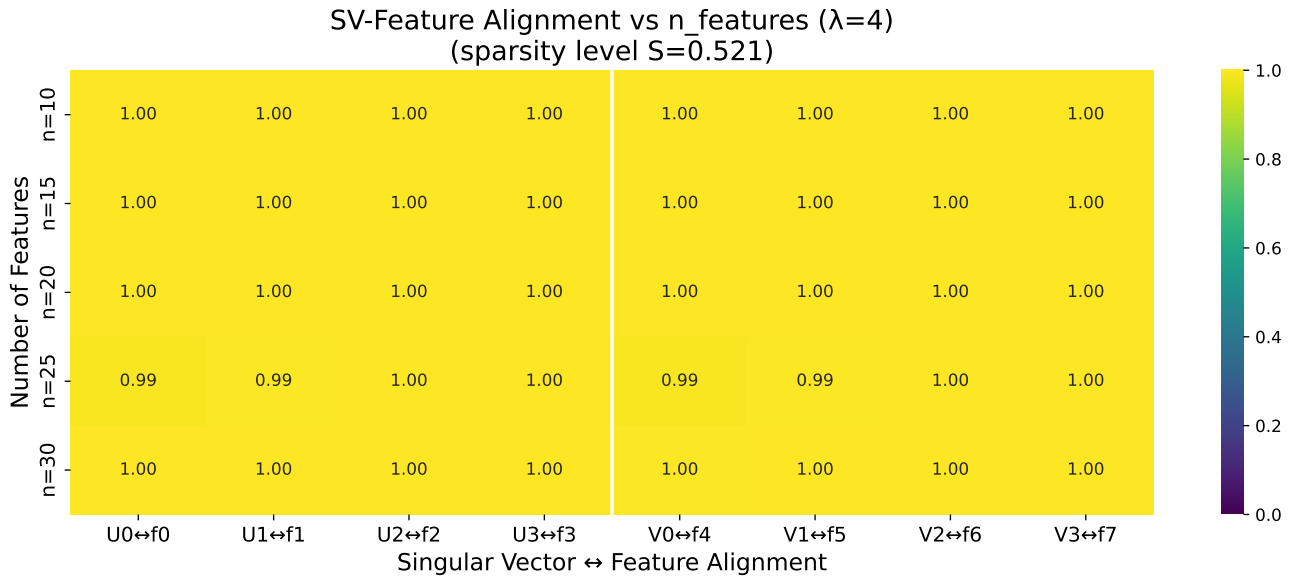
Figure 10 shows that under default settings, alignment occurs robustly across a range of feature sparsities, down to 0.038. At the level of 0.038 or less, feature pairs do not occur often enough in the input for the model to optimize for them. For example, at the level of $p = 0.02$, a given feature pair will only occur in less than 1% of inputs. Figure 11 demonstrates that alignment occurs more readily during training when features are present more often.

Loss Weight λ . The hyperparameter λ is the weight of $\mathcal{L}_{\text{attn}}$ in the model’s loss function and so controls the relative importance of reconstruction loss versus attention loss in training the model. Figure 12 shows that SVF alignment is robust over a range of λ values spanning two orders of magnitude.

Number of Features. There are three dimensional parameters in the model: the number of features N , the hidden dimension D , and the dimension of the attention head H . We study a range of settings by holding the hidden dimension fixed and varying the other two.

First we show that when the number of features varies from the size of the hidden dimension up to three times its size, SVF alignment robustly occurs. Figure 13 shows SVF alignment for $N = 10, 15, 20, 25, 30$.

Head Dimension. Next we show that our results are consistent across varying dimension of the attention head. The head’s dimension must be less than or equal to the hidden dimension, so we study configurations in which head dimension is 10, 8,


 Figure 12. SVF Alignment is robust to λ .

 Figure 13. SVF Alignment is robust to varying number of features (compared to $D = 10$).

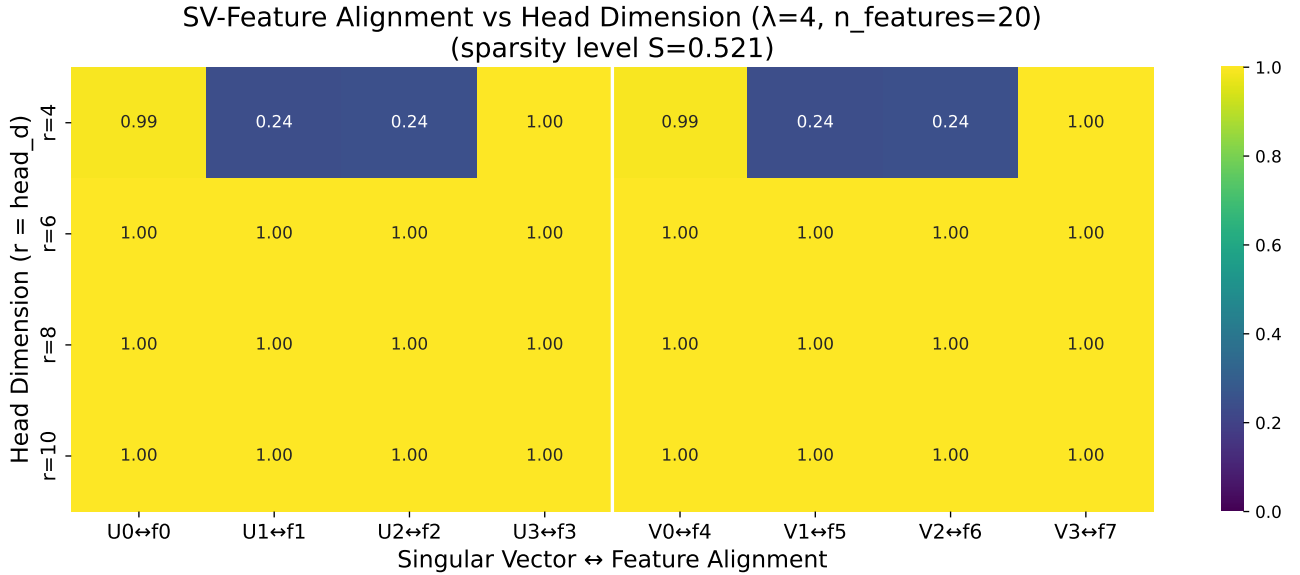


Figure 14. SVF Alignment is robust to varying head dimension (compared to $D = 10$).

6, and 4. Figure 14 shows SVF alignment occurs robustly here as well.

Context Length. The model applies Softmax to logits over a context of size m . Figure 15 shows that SVF alignment occurs over a range of context lengths.

Random Seeds. Finally, in Figure 16 we show that SVF alignment reliably occurs over 5 random seeds.

B. Theoretical Results

B.1. Roadmap to the Theorems

In this section we present theorems that support the experimental results in Section 4.

The first set of theorems (1 - 3) show alignment of singular vectors when features are fixed, attention weights Ω are allowed to vary, and a single feature pair (x_1, y_1) is of interest to the head.

Theorem 1 shows that Ω will be rank-1, and it shows the form that the singular vectors take, which depends on (x_1, y_1) and the covariance of features.

Theorem 2 shows that if features are in isotropic position (also called a tight frame), then the top singular vectors of Ω will exactly align with the features (x_1, y_1) .

Theorem 3 shows that if the features deviate from isotropic position by a small amount, the top singular vectors will still be directionally close to (x_1, y_1) .

Theorem 4 considers the alternative case: attention weights Ω are fixed, features are allowed to vary. Here, there is a reconstruction loss penalty on the features (as in our model).

Theorem 4 shows that if two feature pairs are of interest to the model, and the first feature pair is already aligned with singular vectors of Ω , the second feature pair will be induced to be orthogonal to the first feature pair.

Together, these theorems provide basic theoretical justification for the phenomena observed in Section 4: alignment of features with singular vectors, and orthogonality of aligned features.

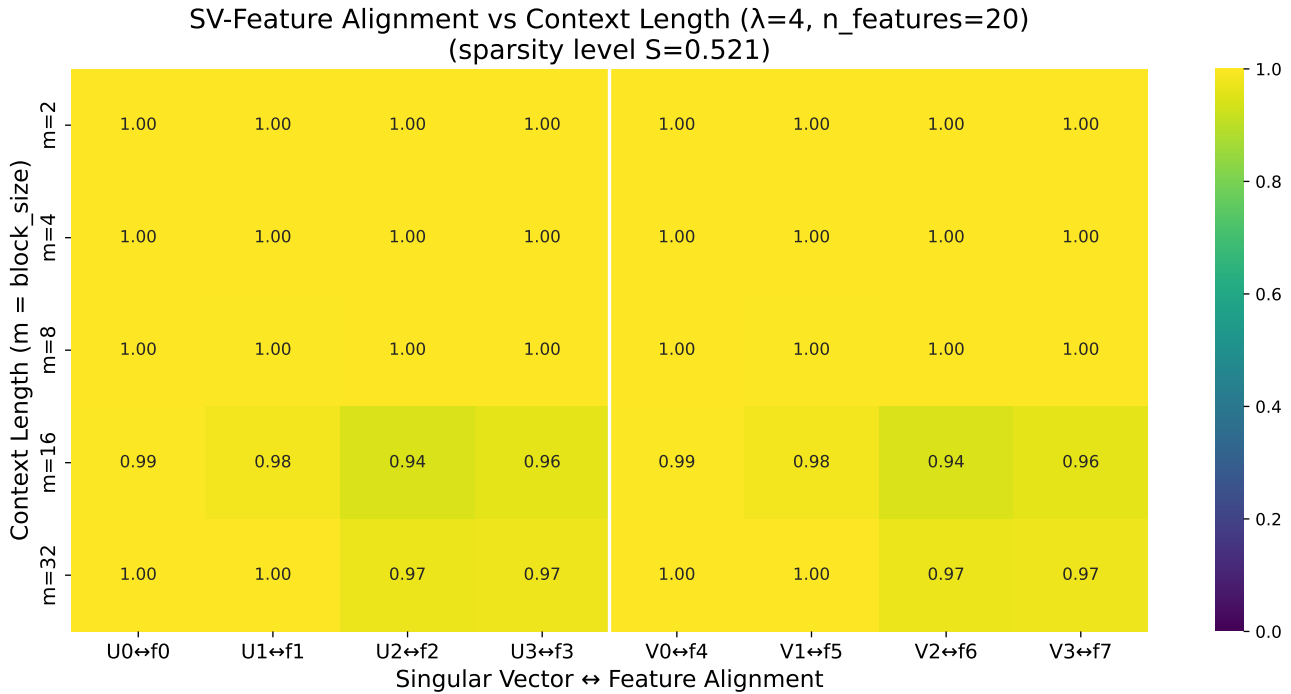


Figure 15. SVF Alignment is robust to varying context length.

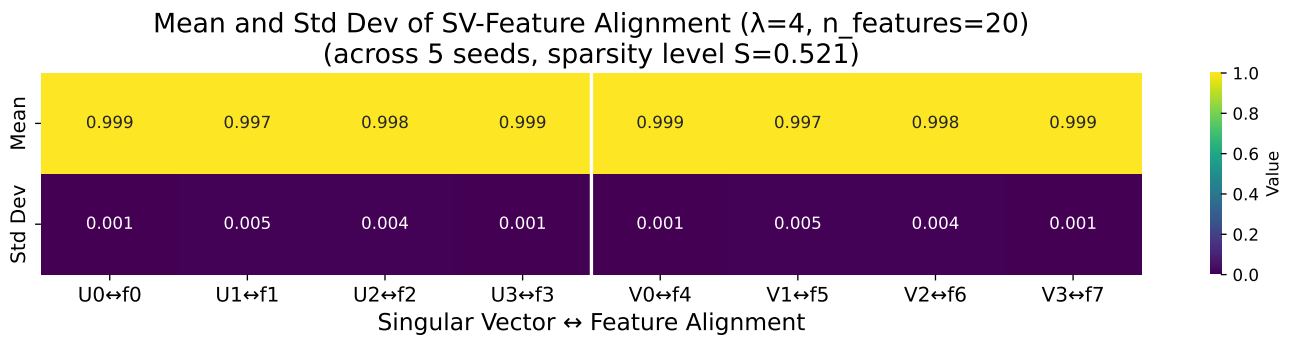


Figure 16. SVF Alignment is robust across a set of random seeds.

B.2. Analysis of SVF Alignment

Features. In our toy model, we considered a single set of features $\{w_i\}$ which could appear in either the query or the key tokens. However, since Ω matrices are not in general symmetric, it is more general to allow the sets of features in the two tokens to differ. So in our theoretical analysis we allow the sets of features appearing in the two tokens to differ, denoting the features appearing in the query token as $\{x_i\}$ and the features appearing in the key token as $\{y_i\}$.

Hence, let $X = x_1, \dots, x_N \subset \mathbb{R}^D$ and $Y = y_1, \dots, y_N \subset \mathbb{R}^D$ be collections of unit vectors, which we will refer to as features.

B.2.1. SETTING

We adopt a student-teacher setting, in which the teacher generates the target attention, and the student (model) learns via that attention pattern. We work in the context of a single head having $\Omega = W_Q^\top W_K$.

Define matrices $X = [x_1 \ \dots \ x_N] \in \mathbb{R}^{D \times N}$, $Y = [y_1 \ \dots \ y_N] \in \mathbb{R}^{D \times N}$, and Gram-like matrices

$$\Sigma_X := XX^\top \in \mathbb{R}^{D \times D}, \quad \Sigma_Y := YY^\top \in \mathbb{R}^{D \times D}.$$

Assumption. In the following we assume that Σ_X and Σ_Y are invertible. This is expected given that we are in the regime of more features than dimensions in the hidden space. In a regime where the covariances are not invertible, Σ_X^{-1} and Σ_Y^{-1} can be replaced by the corresponding Moore-Penrose pseudoinverses.

Tokens. Fix a sampling probability $p \in (0, 1)$. Let $X_p \subseteq X$ be a random subset where each x_i is included independently with probability p , and define the **query token**

$$r := \sum_{x \in X_p} x. \quad (3)$$

Define keys analogously: sample m independent subsets $Y_p^{(1)}, \dots, Y_p^{(m)} \subseteq Y$ (each element included i.i.d. with probability p) and define **key tokens**

$$s_j := \sum_{y \in Y_p^{(j)}} y, \quad j = 1, \dots, m. \quad (4)$$

Student head. Let $\Omega \in \mathbb{R}^{D \times D}$ parameterize a single attention head's bilinear score. Define student logits over keys:

$$\ell_j^{(\Omega)}(r, s_{1:m}) := r^\top \Omega s_j, \quad j = 1, \dots, m,$$

and student attention distribution

$$p_\Omega(j \mid r, s_{1:m}) := \frac{\exp(\ell_j^{(\Omega)})}{\sum_{k=1}^m \exp(\ell_k^{(\Omega)})}.$$

Teacher head. The goal of the teacher head is to output an attention value that depends on whether specific feature pairs are present. In our case, we seek to output a large attention value when features (x_1, y_1) are present. These are the analogs of features (w_0, w_1) in Figure 1(b).

In the body of the paper, for intuitive clarity we parameterize the teacher head using logits, defining in the case of Figure 1(b) that the teacher logit should be 1 iff features (w_0, w_1) are present. We capture the setting of Figure 1(b) by defining $T \in \mathbb{R}^{N \times N}$ with $T_{11} = 1$ and $T_{ij} = 0$ everywhere else. Then the teacher head should satisfy:

$$X^\top \Omega Y = T = e_1 e_1^\top.$$

So

$$\Sigma_X \Omega \Sigma_Y = XX^\top \Omega YY^\top = XTY^\top = x_1 y_1^\top.$$

Hence we define the feature detectors

$$u := \Sigma_X^{-1} x_1, \quad v := \Sigma_Y^{-1} y_1.$$

Given that tokens are generated as sums of features, $u^\top r$ is a (whitened) linear statistic that increases when the component x_1 is present in r *despite correlations among features*; likewise $v^\top s_j$ increases when y_1 is present in s_j . Their product is thus a differentiable analog of ‘‘attend iff (x_1, y_1) is present.’’

Fix a scale $\alpha > 0$ and define the teacher matrix

$$\Omega_T := \alpha u v^\top = \alpha(\Sigma_X^{-1} x_1), (\Sigma_Y^{-1} y_1)^\top.$$

Teacher logits are then:

$$\ell_j^{(T)}(r, s_{1:m}) := r^\top \Omega_T s_j = \alpha(u^\top r)(v^\top s_j),$$

and teacher attention distribution is:

$$p_T(j \mid r, s_{1:m}) := \frac{\exp(\ell_j^{(T)})}{\sum_{k=1}^m \exp(\ell_k^{(T)})}.$$

Training objective. The population objective is the cross-entropy of p_Ω and p_T :

$$\mathcal{L}(\Omega) := \mathbb{E}_{r, s_{1:m}} \left[- \sum_{j=1}^m p_T(j \mid r, s_{1:m}) \log p_\Omega(j \mid r, s_{1:m}) \right],$$

where $(r, s_{1:m})$ are constructed via (3) and (4).

B.2.2. LEMMAS

Lemma 1. *Let $a, b \in \mathbb{R}^m$. Then*

$$\text{softmax}(a) = \text{softmax}(b) \iff a = b + c\mathbf{1} \text{ for some scalar } c \in \mathbb{R},$$

where $\mathbf{1} \in \mathbb{R}^m$ is the all-ones vector.

Proof. If $a = b + c\mathbf{1}$, then $\exp(a_i) = e^c \exp(b_i)$, and normalization cancels e^c . Conversely, if $\text{softmax}(a) = \text{softmax}(b)$, then for all i, j ,

$$\frac{e^{a_i}}{e^{a_j}} = \frac{e^{b_i}}{e^{b_j}} \Rightarrow a_i - a_j = b_i - b_j,$$

which implies $a = b + c\mathbf{1}$. □

Lemma 2. *For any fixed $(r, s_{1:m})$,*

$$-\sum_j p_T(j) \log p_\Omega(j) = H(p_T) + \text{KL}(p_T \| p_\Omega),$$

so $\mathcal{L}(\Omega) = \mathbb{E}[H(p_T)] + \mathbb{E}[\text{KL}(p_T \| p_\Omega)]$.

Proof. Standard identity. □

Lemma 3. *Define differences $d_j = s_j - s_1$ for $j = 2, \dots, m$, and let*

$$\Delta = [d_2 \ \dots \ d_m] \in \mathbb{R}^{D \times (m-1)}, \quad \Sigma_\Delta = \mathbb{E}[\Delta \Delta^\top].$$

Then given that r and s_j are constructed via (3) and (4).

$$\Sigma_\Delta = 2(m-1)p(1-p)\Sigma_Y.$$

In particular, if Σ_Y is invertible, then Σ_Δ is invertible.

Proof. Write each key as

$$s_j = \sum_{i=1}^N a_{j,i} y_i,$$

with $a_{j,i} \sim \text{Bernoulli}(p)$ independent across j, i . Then

$$d_j = s_j - s_1 = \sum_{i=1}^N (a_{j,i} - a_{1,i}) y_i, \quad \mathbb{E}[d_j] = 0.$$

For $j \geq 2$,

$$\mathbb{E}[d_j d_j^\top] = \sum_{i=1}^N \mathbb{E}[(a_{j,i} - a_{1,i})^2] y_i y_i^\top = \sum_{i=1}^N 2p(1-p) y_i y_i^\top = 2p(1-p) \Sigma_Y.$$

Now

$$\Sigma_\Delta = \mathbb{E}[\Delta \Delta^\top] = \sum_{j=2}^m \mathbb{E}[d_j d_j^\top].$$

There are $(m-1)$ terms, so

$$\Sigma_\Delta = 2(m-1)p(1-p) \Sigma_Y$$

So if Σ_Y invertible and $p(1-p) > 0$ and $m \geq 2$, then Σ_Δ is invertible. \square

A similar calculation gives the query second moment

$$\Sigma_r = \mathbb{E}[rr^\top] = p(1-p) \Sigma_X + p^2 m_x m_x^\top, \quad m_x = \sum_{i=1}^N x_i,$$

so Σ_r is invertible whenever Σ_X is invertible and $p \in (0, 1)$.

B.2.3. RESULTS

Theorem 1. Unique Minimizer is Rank-1. *Assume $p \in (0, 1)$, $m \geq 2$, Σ_X and Σ_Y invertible. Then the population objective $\mathcal{L}(\Omega)$ is uniquely minimized at*

$$\Omega^* = \Omega_T = \alpha(\Sigma_X^{-1} x_1)(\Sigma_Y^{-1} y_1)^\top.$$

Consequently, Ω^* is rank-1 and

$$u_1(\Omega^*) \parallel \Sigma_X^{-1} x_1, \quad v_1(\Omega^*) \parallel \Sigma_Y^{-1} y_1.$$

Proof. By Lemma 2,

$$\mathcal{L}(\Omega) = \text{const} + \mathbb{E}[\text{KL}(p_T \| p_\Omega)],$$

so any minimizer must satisfy $\text{KL}(p_T \| p_\Omega) = 0$ almost surely, hence

$$p_\Omega(\cdot \mid r, s_{1:m}) = p_T(\cdot \mid r, s_{1:m}) \quad \text{a.s.}$$

Fix a sample $(r, s_{1:m})$ in this event. By Lemma 1, equality of softmax distributions implies that the corresponding logits differ by a constant shift:

$$r^\top \Omega s_j = r^\top \Omega_T s_j + c(r, s_{1:m}) \quad \forall j.$$

Subtract the equation for $j = 1$:

$$r^\top (\Omega - \Omega_T)(s_j - s_1) = 0 \quad \forall j = 2, \dots, m.$$

In matrix form with $\Delta = [s_2 - s_1 \ \cdots \ s_m - s_1]$,

$$r^\top (\Omega - \Omega_T) \Delta = 0.$$

Multiply by r on the left and by Δ^\top on the right:

$$rr^\top(\Omega - \Omega_T)\Delta\Delta^\top = 0.$$

Take expectations and use independence of r and Δ :

$$\mathbb{E}[rr^\top](\Omega - \Omega_T)\mathbb{E}[\Delta\Delta^\top] = \Sigma_r(\Omega - \Omega_T)\Sigma_\Delta = 0.$$

By Lemma 3, Σ_Δ is invertible (since Σ_Y is invertible, $p \in (0, 1)$, $m \geq 2$). Also Σ_r is invertible (since Σ_X is invertible and $p \in (0, 1)$). Therefore,

$$\Omega - \Omega_T = 0,$$

so $\Omega^* = \Omega_T$ uniquely.

Finally, since $\Omega_T = \alpha uv^\top$ is rank-1, its top left and right singular vectors are proportional to $u = \Sigma_X^{-1}x_1$ and $v = \Sigma_Y^{-1}y_1$. \square

Theorem 2. Exact Alignment. *Assume $p \in (0, 1)$, $m \geq 2$, and the teacher is $\Omega_T = \alpha(\Sigma_X^{-1}x_1)(\Sigma_Y^{-1}y_1)^\top$ with $\alpha > 0$. Further assume that each set of features is in isotropic position (also called a tight frame):*

$$\Sigma_X = aI, \quad \Sigma_Y = bI,$$

for some positive scalars a, b .

Then the unique population minimizer satisfies

$$\Omega^* = \Omega_T = \frac{\alpha}{ab}x_1y_1^\top.$$

In particular, Ω^* is rank-1 and its unique nonzero left and right singular vectors satisfy

$$u_1(\Omega^*) \parallel x_1, \quad v_1(\Omega^*) \parallel y_1.$$

Proof. By Theorem 1 $\Omega^* = \Omega_T$. Under the assumption of isotropy $\Sigma_X^{-1} = \frac{1}{a}I$ and $\Sigma_Y^{-1} = \frac{1}{b}I$, hence

$$\Omega^* = \alpha(\Sigma_X^{-1}x_1)(\Sigma_Y^{-1}y_1)^\top = \alpha \left(\frac{1}{a}x_1 \right) \left(\frac{1}{b}y_1 \right)^\top = \frac{\alpha}{ab}x_1y_1^\top.$$

Thus Ω^* has left and right singular vectors proportional to x_1 and y_1 . \square

Theorem 3. Approximate Alignment. *Let*

$$\Sigma_X = XX^\top = \frac{N}{D}(I + E_X), \quad \Sigma_Y = YY^\top = \frac{N}{D}(I + E_Y), \quad (5)$$

for some symmetric ‘‘error’’ matrices $E_X, E_Y \in \mathbb{R}^{D \times D}$. Assume the sets are close to isotropic with $\max\{\|E_X\|_2, \|E_Y\|_2\} < 1/2$. Define $\tau = 4\|E_X\|_2\|E_Y\|_2 + 2\|E_X\|_2 + 2\|E_Y\|_2$. Then if $\tau < 1$,

$$\sin \angle(u_1, x_1), \sin \angle(v_1, y_1) < \frac{\tau}{1 - \tau},$$

and in particular if $\tau < 1/2$,

$$\sin \angle(u_1, x_1), \sin \angle(v_1, y_1) < 8\|E_X\|_2\|E_Y\|_2 + 4\|E_X\|_2 + 4\|E_Y\|_2. \quad (6)$$

We note that the operator norm bound on E_X also establishes a bound on feature interference, because XX^\top and $X^\top X$ have the same spectra.

Proof. From Theorem 1 the minimizer is

$$\Omega^* = \alpha \Sigma_X^{-1} x_1 y_1^\top \Sigma_Y^{-1}.$$

From (5), we have

$$\Sigma_X^{-1} = \frac{D}{N} (I + E_X)^{-1}, \quad \Sigma_Y^{-1} = \frac{D}{N} (I + E_Y)^{-1}.$$

Therefore

$$\Omega^* = \alpha \left(\frac{D}{N} \right)^2 (I + E_X)^{-1} x_1 y_1^\top (I + E_Y)^{-1}. \quad (7)$$

We will rewrite Ω^* as

$$\Omega^* = \lambda (x_1 y_1^\top + \Delta), \quad \lambda := \alpha \left(\frac{D}{N} \right)^2, \quad (8)$$

where Δ collects all terms that prevent Ω^* from being exactly rank 1 in the direction $x_1 y_1^\top$. Then

$$\Delta = (I + E_X)^{-1} x_1 y_1^\top (I + E_Y)^{-1} - x_1 y_1^\top \quad (9)$$

Defining $A = (I + E_X)^{-1}$ and $C = (I + E_Y)^{-1}$, (9) can be rewritten as

$$\Delta = (A - I) x_1 y_1^\top (C - I) + (A - I) x_1 y_1^\top + x_1 y_1^\top (C - I) \quad (10)$$

To bound Δ in operator norm, an important first step is to bound $\|A - I\|_2$ and $\|C - I\|_2$. Since by assumption $\|E_X\|_2 < 1$ and $\|E_Y\|_2 < 1$, the inverses can be expanded in a Neumann series

$$(I + E_X)^{-1} = I - E_X + E_X^2 - \dots, \quad (I + E_Y)^{-1} = I - E_Y + E_Y^2 - \dots,$$

which converges absolutely in operator norm. So we can bound $\|A - I\|_2$:

$$\|A - I\|_2 = \left\| \sum_{k=1}^{\infty} (-E_X)^k \right\|_2 \leq \sum_{k=1}^{\infty} \|E_X\|_2^k = \frac{\|E_X\|_2}{1 - \|E_X\|_2}$$

and similarly for $\|C - I\|_2$. Since we assume $\|E_X\|_2, \|E_Y\|_2 \leq 1/2$:

$$\|A - I\|_2 \leq \frac{\|E_X\|_2}{1 - \|E_X\|_2} \leq 2\|E_X\|_2. \quad (11)$$

Next, to bound the influence of Δ , we use submultiplicativity of the operator norm applied to (10):

$$\|\Delta\|_2 \leq \|A - I\|_2 \|x_1 y_1^\top\|_2 \|C - I\|_2 + \|A - I\|_2 \|x_1 y_1^\top\|_2 + \|x_1 y_1^\top\|_2 \|C - I\|_2$$

and noting (11) as well as that $\|x_1 y_1^\top\|_2 = 1$:

$$\|\Delta\|_2 \leq 4\|E_X\|_2\|E_Y\|_2 + 2\|E_X\|_2 + 2\|E_Y\|_2. \quad (12)$$

To bound the deviation of the singular vectors of Ω^* from x_1, y_1 , we use a standard singular-vector perturbation theorem. Recalling (8):

$$\Omega^* = \lambda (x_1 y_1^\top + \Delta),$$

let u_1, v_1 be the top left and right singular vectors of Ω^* . Applied to our setting, Wedin's theorem (P.-Å. Wedin, 1972) states that

$$\sin \angle(u_1, x_1) \leq \frac{\|\Delta\|_2}{\delta} \quad (13)$$

where $\delta = \sigma_1(x_1 y_1^\top) - \sigma_2(x_1 y_1^\top + \Delta)$. Weyl's inequality Horn & Johnson (2012, Theorem 4.3.1) shows that $|\sigma_2(x_1 y_1^\top) - \sigma_2(x_1 y_1^\top + \Delta)| \leq \|\Delta\|_2$, so $\delta \geq 1 - \|\Delta\|_2$. So as long as $\|\Delta\|_2 < 1$,

$$\sin \angle(u_1, x_1), \sin \angle(v_1, y_1) < \frac{\|\Delta\|_2}{1 - \|\Delta\|_2}$$

and in particular if $\|\Delta\|_2 \leq 1/2$, then

$$\sin \angle(u_1, x_1), \sin \angle(v_1, y_1) < 8\|E_X\|_2\|E_Y\|_2 + 4\|E_X\|_2 + 4\|E_Y\|_2.$$

□

B.3. Feature Orthogonalization

Next we show that when features vary and Ω is fixed, interference between features will result in orthogonalization of features.

B.3.1. SETTING

For clarity we analyze the setting with two X features (x_1, x_2) and two Y features (y_1, y_2) . The query token r can be either x_1 or x_2 , and the key token can be either y_1 or y_2 . We assume that SVF alignment has taken place for features (x_1, y_1) , meaning that the top singular vectors of Ω are $(u_1, v_1) = (x_1, y_1)$. We will show that under these conditions, if (x_2, y_2) are allowed to vary, they will become orthogonal to (u_1, v_1) .

Since there are only two possible key tokens, softmax reduces to a sigmoid on a logit gap $\delta := \ell_1 - \ell_2$. In the two-token case, $p_\Omega(1) = \sigma(\delta)$ with $\sigma(t) = \frac{1}{1+e^{-t}}$. The teacher sets a probability p^* and training uses two-key cross-entropy:

$$\text{CE}(p^*, \sigma(\delta)) = -p^* \log \sigma(\delta) - (1 - p^*) \log(1 - \sigma(\delta)). \quad (14)$$

We assume the teacher matrix is rank-2:

$$\Omega_T = \sigma_1 u_1 v_1^\top + \sigma_2 u_2 v_2^\top, \quad \sigma_1 > \sigma_2 > 0, \quad (15)$$

with orthonormal u_1, u_2 and v_1, v_2 .

Note that $(x_1, y_1) = (u_1, v_1)$. Let x_2, y_2 be trainable unit vectors. We consider two contexts, each with two key tokens $s_1 = y_1$ and $s_2 = y_2$. In each context, we define the *teacher gap* δ^* which is the difference of logits between $r^\top \Omega y_1$ and $r^\top \Omega y_2$. This is the parameterization of the attention head.

We focus on establishing the orthogonality of y_2 and y_1 .

To capture the need for accurate reconstruction of inputs, we penalize interference between features. Thus our overall training objective is

$$\mathcal{J}(x_2, y_2) = \text{CE}(\delta_A^*, \delta_A(x_2, y_2)) + \text{CE}(\delta_B^*, \delta_B(x_2, y_2)) + \frac{\lambda}{2} (y_2^\top y_1)^2 \quad (16)$$

where the student gaps are

$$\delta_A(x_2, y_2) = x_1^\top \Omega_T (y_1 - y_2), \quad \delta_B(x_2, y_2) = x_2^\top \Omega_T (y_1 - y_2)$$

B.3.2. RESULTS

Theorem 4. CE minimization with reconstruction loss forces orthogonalization. *Let $(x_2^\lambda, y_2^\lambda)$ be any global minimizer of (16), with the constraints $\|x_2\| = \|y_2\| = 1$. Then*

$$y_2^{\lambda\top} y_1 \leq \sqrt{\frac{2}{\lambda} \left(\mathcal{J}_\lambda(x_2', y_2') - \inf_{x_2, y_2} [\text{CE}(\delta_A^*, \delta_A(x_2, y_2)) + \text{CE}(\delta_B^*, \delta_B(x_2, y_2))] \right)}$$

for any comparison pair (x_2', y_2') with $\|x_2'\| = \|y_2'\| = 1$. In particular, if there exists a feasible (x_2', y_2') achieving minimal CE while also having $y_2'^\top y_1 = 0$, then the optimizer must satisfy $y_2^{\lambda\top} y_1 = 0$

Proof. Fix any $\lambda > 0$. For any (x_2, y_2) we can decompose the objective as

$$\begin{aligned} \mathcal{J}(x_2, y_2) &= \underbrace{\text{CE}(\delta_A^*, \delta_A(x_2, y_2)) + \text{CE}(\delta_B^*, \delta_B(x_2, y_2))}_{=: \mathcal{L}_{\text{CE}}(x_2, y_2)} + \frac{\lambda}{2} (y_2^\top y_1)^2 \end{aligned}$$

Let $(x_2^\lambda, y_2^\lambda)$ be a global minimizer.

Now choose any comparison pair (x_2', y_2') with $y_2'^\top y_1 = 0$. Optimality gives

$$\mathcal{L}_{\text{CE}}(x_2^\lambda, y_2^\lambda) + \frac{\lambda}{2} (y_2^{\lambda\top} y_1)^2 \leq \mathcal{L}_{\text{CE}}(x_2', y_2') + \frac{\lambda}{2} \underbrace{(y_2'^\top y_1)^2}_{=0}.$$

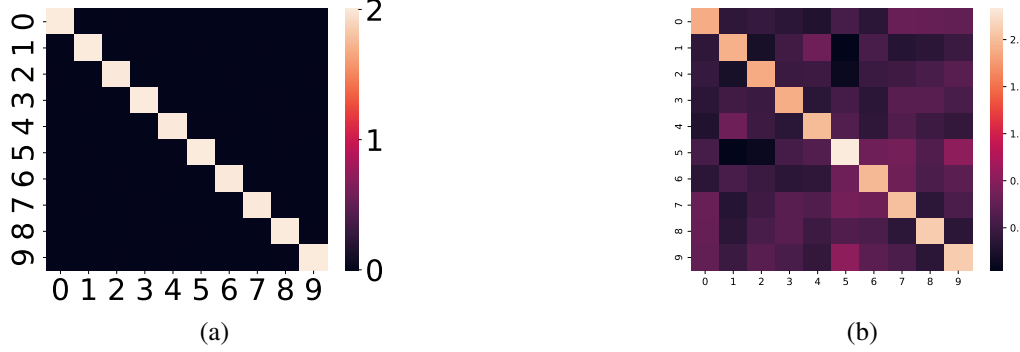


Figure 17. WW^\top matrices showing isotropic arrangement of features (a) without attention, and (b) when two features are of interest to the head.

Rearranging yields the finite- λ bound

$$\frac{\lambda}{2}(y_2^{\lambda^\top} y_1)^2 \leq \mathcal{L}_{\text{CE}}(x'_2, y'_2) - \mathcal{L}_{\text{CE}}(x_2^\lambda, y_2^\lambda) \leq \mathcal{L}_{\text{CE}}(x'_2, y'_2) - \inf_{x_2, y_2} \mathcal{L}_{\text{CE}}(x_2, y_2)$$

which establishes the result. \square

C. Isotropy

Here we show evidence of the isotropy of features in the toy model. We consider two cases, corresponding to Figures 1(a) and (b). In Figure 17(a) we show WW^\top for the case where no attention head is present. The figure shows that the features are arranged isotropically. In Figure 17(b) we show WW^\top for the case where two features are of interest. Here, features are still arranged approximately isotropically, suggesting that the requirements of Theorems 2 and 3 for subsequent SVF alignment can still be met over the remaining features.

D. More Features of Interest than Head Capacity

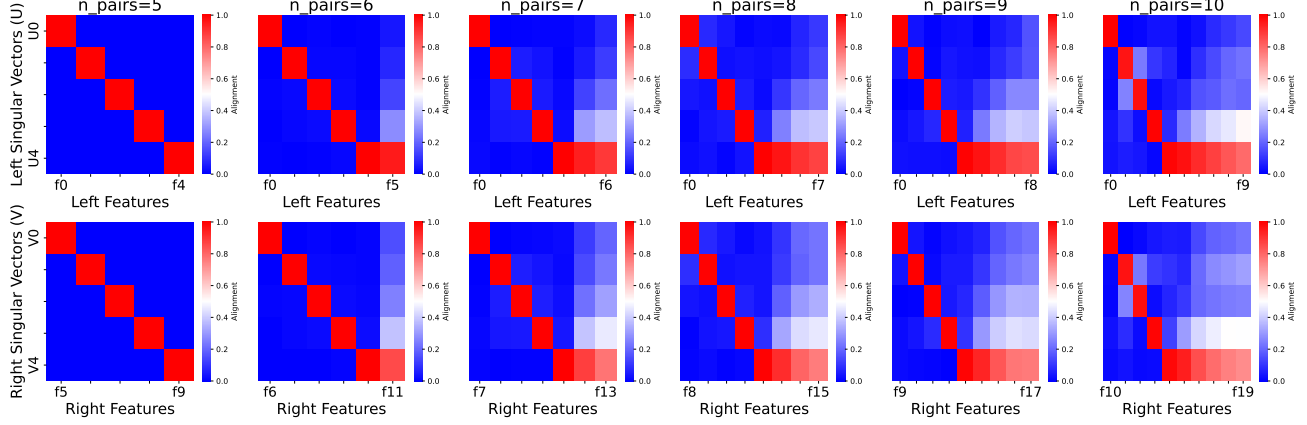
Here we present a preliminary study of the nature of SVF alignment when there are more features of interest to the head than can be represented orthogonally in \mathbb{R}^H . The experiments in Section 4 show that the toy model assigns one feature pair to each singular vector direction. However, when the number of feature pairs is greater than H , this is no longer possible because the rank of Ω is H .

To study this setting we constrain the representational capacity of the head by setting $H = 5$. We then study the case in which the number of features of interest ranges from H (5) to $2H$ (10). As usual, the target logits decline linearly with the pair index. Here, ℓ^T of pair i is set to $1 + \text{the number of features} - i$.

In Figure 18(a), we show alignment of the five singular vectors of the head with the features for each case. Surprisingly, the model assigns all of the features having the lowest target logits to the smallest singular vector (singular vector with the smallest singular value). Figure 18(b) shows that this effect persists when we model capacities are higher ($H = 10$, features of interest range from 10 to 20).

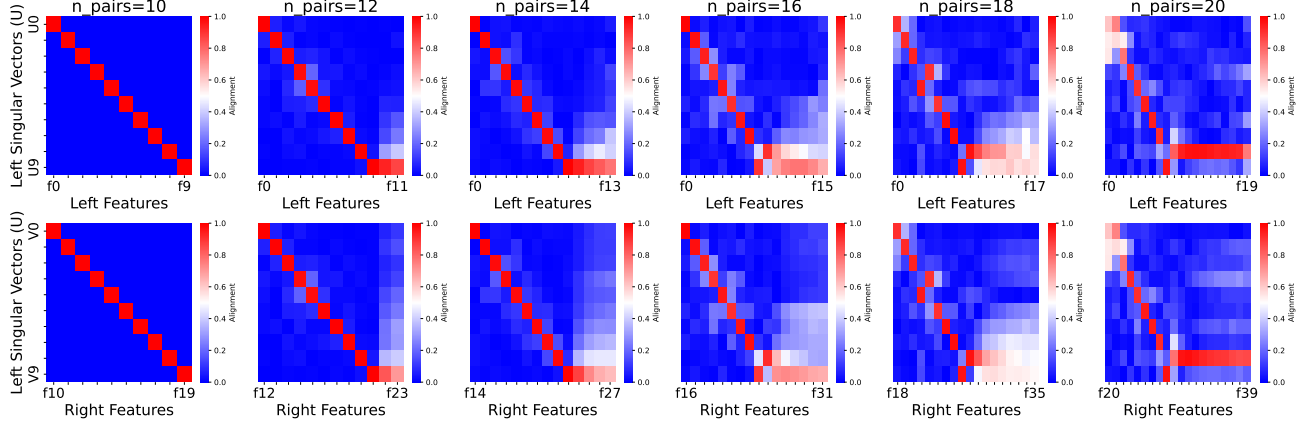
This behavior has a number of consequences. It means that the model cannot distinguish the features that mapped to the same singular vector, and in fact can mistakenly associate features from different pairs. On the other hand, the model still allocates high-logit features one-to-one with singular vectors. As a result, most singular vectors of the model still correspond to features. We note that sparse decomposition will still arise for a model in this setting, although less robustly.

Clearly, more study is needed to understand the behavior of SVF alignment when the number of features of interest to the head exceeds its capacity, but these results give an initial indication that SVF alignment still can have utility in this regime.



(a) $N = 20$ features, hidden dimension $D = 10$, head dimension $H = 5$.

Number of feature pairs of interest varies from 5 (head capacity) to 10 (model capacity).



(b) $N = 40$ features, hidden dimension $D = 20$, head dimension $H = 10$.

Number of feature pairs of interest varies from 10 (head capacity) to 20 (model capacity).

Figure 18. When there are more features of interest than head capacity, features are superposed primarily on the smallest singular vector, and most singular vectors still map to a single feature. Absolute cosine similarity of features and singular vectors. We show absolute value of cosine similarity for clarity due to sign ambiguity of SVD.

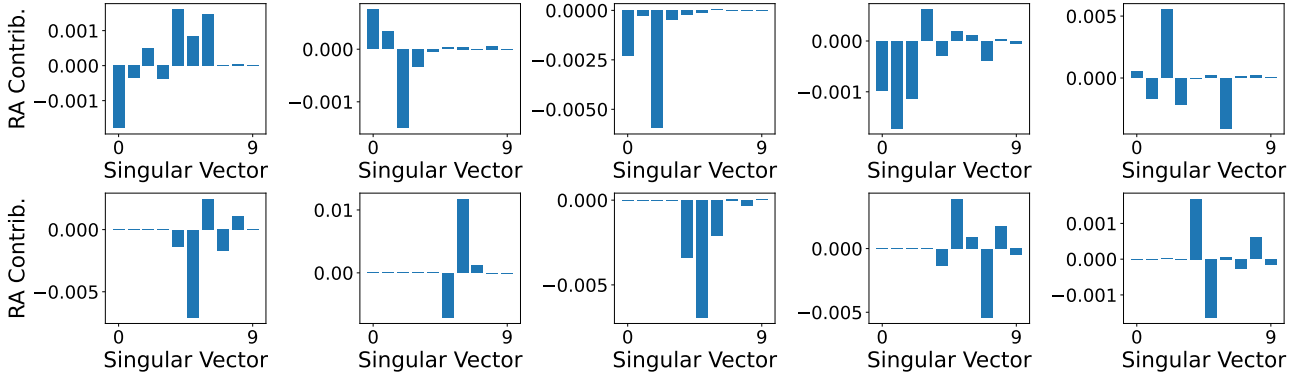


Figure 19. When features of interest are not present, attention is not sparsely decomposable. Top: Token pairs without features of interest, early in training; Lower: Late in training. Compare to Figure 4.

E. Sparse Attention Decomposition in Toy Model Indicates that Features of Interest are Present

Here we show that in the toy model, sparse attention decomposition occurs only when at least one feature pair of interest is present. To show this, we consider the complementary case to Figure 4. Figure 19 shows that when features of interest are *not* present, sparsity of attention decomposition is *absent*.

F. Pythia Experiments

F.1. Details of Experiments

Here we provide details of our study of sparse attention decomposition in Pythia (Section 5). We used the following prompt from the Indirect Object Identification task (Tigges et al., 2024): *Then, Simon and Andrew were working at the restaurant. Simon decided to give a basketball to.* The highest-logit output token is “Andrew”, indicating that the model successfully completes the task.

We denote the tokens that participate in the circuit as follows: ‘Simon’: S1; ‘and’: S1+1; ‘Andrew’: IO; ‘Simon’ (second occurrence): S2; and ‘to’ (second occurrence): END. We use the heads and token pairs identified as participating in the circuit by (Tigges et al., 2024). Table 2 lists the heads and token pairs used.

Our results in Figures 6(b) and 8(b) are averaged over the heads in Table 2, and smoothed with a window size of 8.

Name	Layer	Head	Destination Token	Source Token
Previous Token	2	6	S1+1	S1
Induction 1	4	11	S2	S1+1
Induction 2	4	6	S2	S1+1
Induction 3	5	0	S2	S1+1
Name Mover 1	10	7	END	IO
Name Mover 2	9	4	END	IO
Name Mover 3	8	2	END	IO
Name Mover 4	8	10	END	IO
S-Inhibition 1	7	9	END	S2
S-Inhibition 2	6	6	END	S2
S-Inhibition 3	7	2	END	S2
Positive Copy Suppression 1	8	9	END	S2

Table 2. Attention heads used in studying Pythia, Section 5

F.2. Relative Attention Sparsifies as a Result of Training

In Figure 20 we present relative attention decompositions for all of the heads studied in Pythia, at the start and end of training. These heads and token pairs were identified as participating in the IOI circuit in (Tigges et al., 2024).

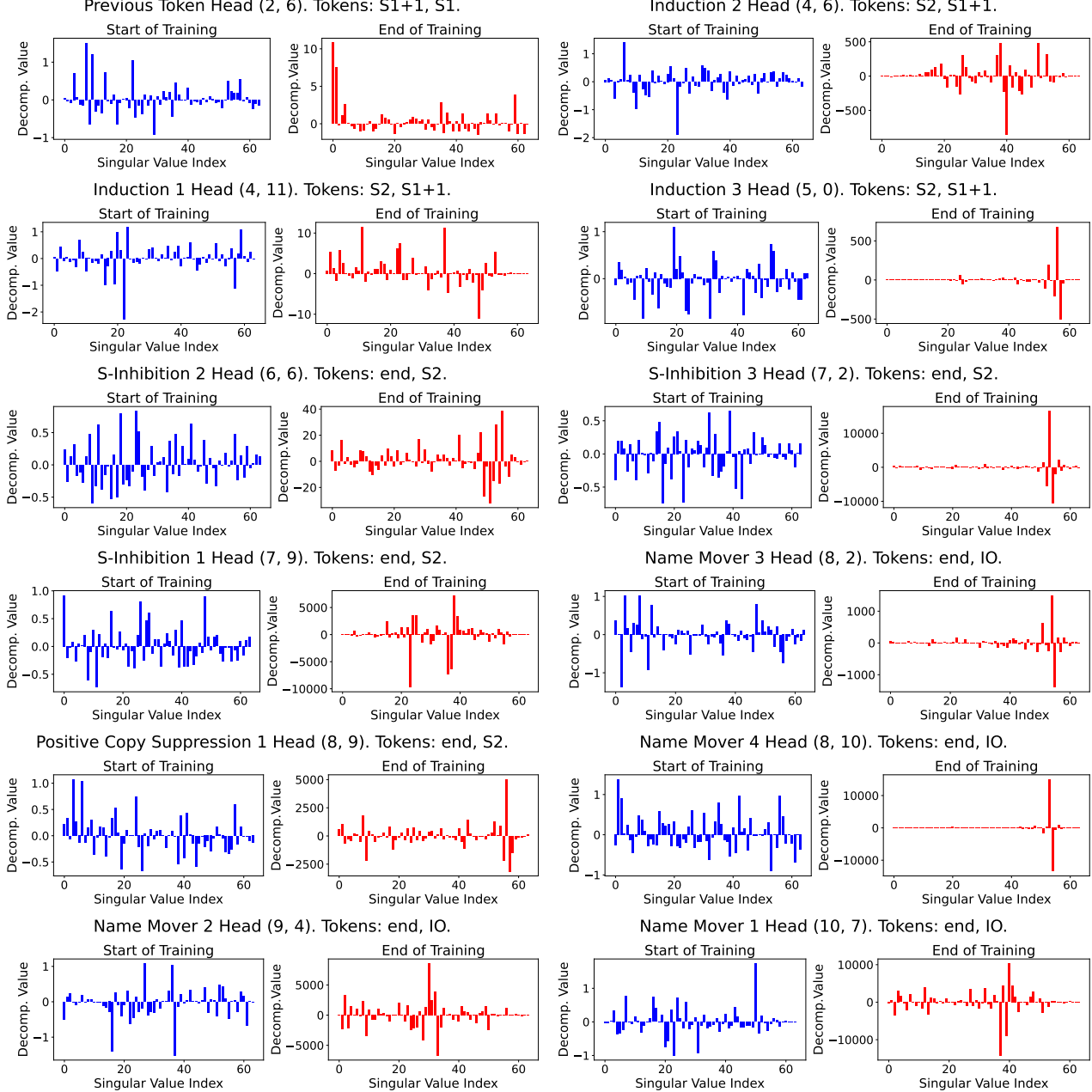


Figure 20. Sparse decomposition in Pythia generally increases during training. Each plot shows decomposition of relative attention at the start and end of training.